PERSPECTIVE • OPEN ACCESS

Opportunities and challenges for direct electrification of chemical processes with protonic ceramic membrane reactors

IOP Publishing Prog. Energy 6 (2024) 043007 https://doi.org/10.1088/2516-1083/ad80f4

Progress in Energy

OPEN ACCESS

RECEIVED
11 February 2024

REVISED
26 July 2024

ACCEPTED FOR PUBLICATION
27 September 2024

PUBLISHED
15 October 2024

PERSPECTIVE

Opportunities and challenges for direct electrification of chemical processes with protonic ceramic membrane reactors

Nannan Li[1], **Athanasios Zarkadoulas**[1] **and Vasileios Kyriakou**[*]

Engineering and Technology Institute Groningen (ENTEG), University of Groningen, Nijenborgh 4, 9747 AG Groningen, The Netherlands

[1] These authors contributed equally to this work.

[*] Author to whom any correspondence should be addressed.

E-mail: v.kyriakou@rug.nl

Keywords: electrification, protonic ceramic cells, electrochemical membrane reactors, electroconversion, (de)hydrogenation

Abstract

The necessity of developing sustainable energy storage and process electrification technologies has built an unprecedented momentum for protonic ceramic membrane reactors (PCMRs). PCMRs are practically electrolytic cells (or even fuel cells in case of cogeneration) that extend beyond the classical approach of electrolysis towards producing a variety of value-added chemicals or fuels. The use of a ceramic electrolyte membrane to electrochemically supply or remove hydrogen offers unique advantages, such as process intensification, cogeneration of chemicals and electricity, as well as the shift of the chemical equilibrium to the desired products. During the last few years, rapid progress has not only been made in the cell components, but also for upscaling, which reveals their high potential in terms of efficiency and flexibility. Herein, we discuss recent innovations and breakthroughs in the PCMR concepts and components for different processes, while we attempt to identify challenges that may hinder their wide deployment. Closer to commercialization is the production of pressurized hydrogen from sustainable sources, i.e. biogas and ammonia, while significant advancements have been made in reversible H_2O electrolysis systems. CO_2/H_2O co-electrolysis, hydrocarbon conversion and ammonia synthesis have been also successfully demonstrated, albeit with different obstacles related to the product selectivity and stability of the cell reactors. We conclude that future projects should target beyond the experimental discovery of materials, such as, multiscale modeling that would aid optimization of the involved surfaces, interfaces, and the operating parameters towards enhancing the viability of electrosynthesis in PCMRs.

1. Introduction

As a major contributor to the global greenhouse emissions, the commodity chemical industry should be modernized by being coupled with renewable electricity and neutral carbon sources to gain independence from fossil fuels. Electrification of the chemical industry through Power-to-X (X: chemicals or fuels) technologies is considered one of the promising solutions for a sustainable future by offering unique advantages for the production of valuable commodity chemicals from abundant feedstocks, such as carbon dioxide, water (and steam), dinitrogen, biomass or biogas with high efficiency at milder conditions [1–5]. These environmentally friendly but in practice impossible reactions for thermochemical reactors (e.g. for water splitting) are enabled through the direct transduction of electrical power to chemical bonds [6]. Besides the important process advantages due to direct electrification, solutions for grid-scale electricity storage and bulk transport (e.g. pipelines or sea) of renewable power as chemical energy are also enabled in such paradigms [3].

Electrochemical energy storage, as currently realized in modern fuel cells and electrolyzers, is compact, modular and quiet, which renders relative systems attractive for energy storage approaches. Electrochemical Membrane Reactors are practically electrolysis cells (or fuel cells in case of cogeneration) that extend beyond

the classical approach of water splitting and they can exhibit increased yields towards production of useful chemicals or/and electrical energy [7–9]. EMRs consist primarily of an electrolyte membrane, which allows the *in-situ* supply or removal of one of the reactants or products, respectively from/to a separate chamber in the form of an ion. This offers several advantages, such as the simultaneous production and separation of a useful product (e.g. hydrogen) in a single device, cogeneration of chemicals and electricity, as well as the shift of the chemical equilibrium to the desired products [7–11].

To this direction, EMRs which employ a solid electrolyte ceramic membrane as their main component have gained significant interest due to their structural and mechanical stability at high temperatures at which higher efficiencies can be obtained and industrially relevant reactions take place [10–13]. Solid electrolytes belong to the general category of inorganic dense membranes [11]. The ceramic electrolyte is routinely sandwiched between two solid porous electrodes, allowing the exchange of various ionic species e.g. O^{2-}, H^+, Na^+, Li^+, etc. Of particular interest are the membranes that conduct O^{2-} and H^+ species since most of the reactions in chemical industry involve oxidations and (de)hydrogenation processes, providing an exciting platform for innovation in the field of electrification. Several recent and older reviews have described the use of oxide ion and proton conductors from the solid oxide electrolyzers perspective [14–19] but here we are focusing on the potential of the EMRs for chemical conversion.

The discovery of high temperature proton conductors by Iwahara *et al* [20, 21] in the early 80 s enabled the construction and development of the first high temperature solid state protonic electrochemical cells. Since then, numerous materials have been discovered [22–24] that exhibit proton (H^+) conductivity at elevated temperatures (400 °C–700 °C) having significant applications for chemical processes due to the exchange of electrochemical hydrogen in critical (de)hydrogenation reactions. The first works on chemical reactors were carried out in the 90 s and the 00 s with the first reports being on methane activation, ammonia synthesis at atmospheric pressure, hydrocarbon dehydrogenation and electrochemical promotion of catalysis [13, 25–27].

However, it was not until the last decade that the protonic membrane manufacturing took a great boost due to the development of high conductivity cells based on mixed NiO-$BaZrO_3$-$BaCeO_3$ oxides with tubular or planar geometry of low thickness [28–33]. The $BaZr_{1-x-y}Ce_xY_yO_{3-\delta}$(BZCY) electrolyte films are typically supported on a porous Ni-BZCY support, which concurrently serves as one of the electrodes. Such cells allow significant protonic fluxes with high transport numbers, exhibit appreciable mechanical strength and chemical stability, and have thus been the main component of proton ceramic membrane reactors (PCMRs) [26, 34–38]. In the present work, we discuss important innovations and breakthroughs in electrode and electrolyte materials, as well as concepts or designs in the different catalytic processes (figure 1), namely:

(a) Steam electrolysis for green hydrogen production
(b) Carbon dioxide valorization to value added chemicals/fuels
(c) Methane (or biogas) activation to olefins, aromatics and syngas
(d) Ethane and Propane dehydrogenations
(e) Ammonia synthesis and decomposition for green hydrogen storage

We also attempt to confront the challenges that hinder their wide deployment, while an effort is given to identify solutions for overcoming these hurdles. The last part of this work discusses opportunities, directions and possible dead ends for the PCMR technologies with the overall objective to identify key, recent, and authoritative references for the reader to delve further into.

2. The heart of the PCMR: the proton conducting electrolyte

The solid electrolyte is one of the building blocks of PCMRs along with anodic and cathodic electrocatalysts. It has a significant impact on the cell performance since it will determine the proton flux and therefore, the hydrogen supply or pumping rate during the electrochemical reactions. To this end, the candidate materials should possess high ionic conductivity with negligible electronic conductivity to avoid electron leakage. The electrolyte should also be highly dense to hinder possible gas crossover between the anodic and cathodic chambers that will have an impact on the open-circuit voltage. Chemical stability under various operation conditions, such as oxidizing and/or reducing environments, as well as steam and/or carbon-containing gas atmospheres accompanied with chemical compatibility with the neighboring electrocatalysts are of essence.

Since the pioneering works of Iwahara and co-workers, different crystal structures including perovskites, ortho-phosphates, ortho-niobates and ortho-tantalates have been proposed as protonic electrolytes [22]. Apart from BZCY-type electrolytes, different oxides have also been reported to offer promising proton conductivity <600 °C. Among them, lanthanum tungstate (LWMO) [38], F-doped LWMO

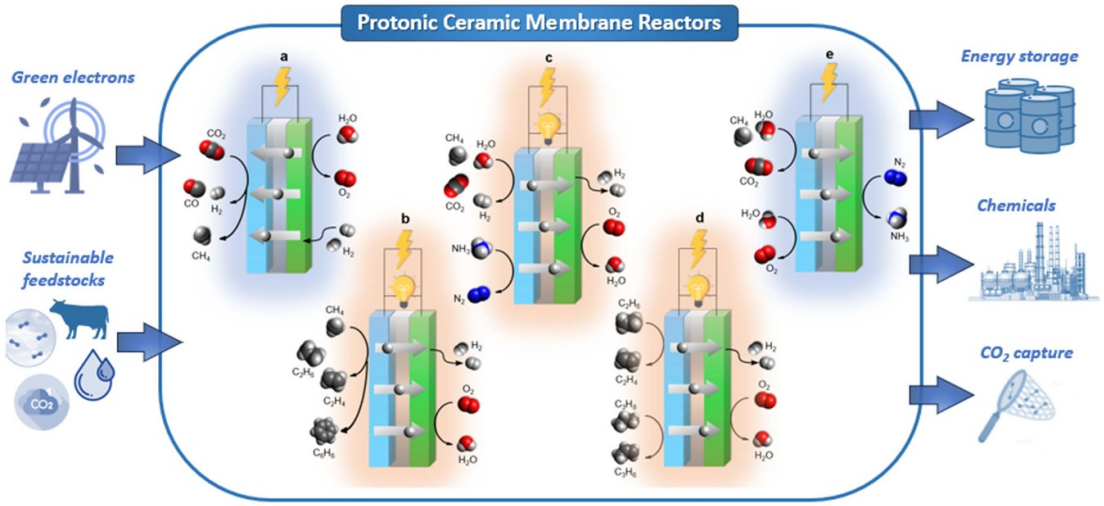

Figure 1. Concepts studied in PCMRs. (a) Steam electrolysis and CO_2/H_2O co-electrolysis, (b) methane activation, (c) hydrogen extraction or power generation from renewable hydrogen sources, (d) alkane to alkene conversion and (e) ammonia synthesis. The orange fading color represents the opportunity of cogeneration of electricity by operating the reactor in fuel cell mode.

($La_{5.5}W_{0.6}Mo_{0.4}O_{11.25-\delta}F_x$) [39, 40], Cl-doped LWMO [41] showed satisfying hydrogen permeability and stability.

Till today, ABO_3 perovskites are the ones with the widest deployment due to their low activation energy for proton transport [24]. Proton transport requires local defects in the solid, such as oxygen vacancies in order to react with steam and produce protons through the hydration reaction:

$$H_2O_{(g)} + V_O^{\cdot\cdot} + O_o^x \rightarrow 2OH_O^{\cdot} \quad (1)$$

where $V_O^{\cdot\cdot}$, O_o^x and $OH_O^{\cdot}$ represent oxygen vacancy, lattice oxygen, and proton, respectively [42]. In addition, the Grotthuss mechanism suggests that formed protons reorient to a lattice oxygen, and then hop to the nearest oxygen ion through an OH–O bond formation. These mechanisms indicate that the local $V_O^{\cdot\cdot}$ concentration and the proton mobility rate determine the proton conductivity of perovskite oxides (PO) [43]. Based on these considerations, $BaZrO_3$ theoretically displays the highest bulk proton conductivity due to its higher symmetry and unit cell volume of the crystal which are combined with high chemical and structural stability [22, 24, 32, 33, 44]. Nonetheless, different experimental findings showed that the acceptor-doped $BaCeO_3$ displays the highest H^+ fluxes due to lower grain boundary resistance and better sinterability, but with much lower chemical stability under H_2O and CO_2 atmospheres. Hence, by successfully mixing these two oxides $(Ba(Zr,Ce))O_3$, a trade-off solution between conductivity ($\sim$10 mS cm^{-1} in humidified atmospheres) and the chemical/mechanical structure is stabilized by doping yttrium oxide [34, 45, 46].

Several efforts towards maximizing the proton conductivity and the sinterability of such oxides have been reported, either by optimizing the Ce/Zr ratio or attempting alternative B-site doping strategies or the addition of sintering agents (e.g. NiO or ZnO) [47]. Another interesting advancement was the doping of Yb which has been reported to increase the total conductivity and stability under carbon-rich conditions [47]. However, further experimental work is still required to draw conclusive arguments by elucidating the relationship of the structural and chemical properties of these materials with their observed performance. The above-mentioned works are clear evidence of the significant progress in the discovery and optimization of BZCY and BZCYYb materials that enabled protonic ceramic electrolytes to reach the required protonic fluxes to compete with the oxide ion SOECs.

3. Geometry considerations

Planar and tubular cell configurations are related to the development and operation of all types of solid oxide cells, including protonic ceramic reactors. The choice of cell geometry has implications on various factors, such as the conversion, product selectivity, heat dissipation and management, etc. Briefly, a planar cell exhibits a sandwich-like structure, with the dense electrolyte layer in the middle separating the anode and cathode porous layers. The dense structure of the electrolyte ensures separation of the two (porous) anode and cathode chambers and provides proton conductivity. In a proton-conducting solid oxide cell, steam is

converted to protons and oxygen (air electrode), protons transfer across the electrolyte and undergo further reactions at the other side of the cell (fuel electrode). The planar structure is the most prevalent design, since it offers the benefits of lower cost, straightforward assembly, short paths for current transport, and high output powers. However, it faces challenges regarding sealing (affecting gas-tightness) and thermal stability. Tubular configurations, on the other hand, can offer a viable alternative for sealing problems, increased scalability (stack size), improved heat distribution, but typically display lower power densities due to the higher complexity in current collection [47].

4. Reactions in PCMRs

4.1. Steam electrolysis for green hydrogen production

In PCMRs the steam electrolysis to its elements (typically called protonic ceramic electrolysis cells—PCECs when H_2O electrolysis is involved) is the most extensively studied reaction system since it offers highly efficient storage of intermittent renewable electricity as hydrogen for later use in energy applications or chemical industry. In PCEC, the steam splits at the anode (positrode) simultaneously with the oxygen evolution reaction (OER), while the molecular hydrogen is recovered at the cathodic electrode (negatrode) side:

$$\text{Anode:} \quad 2H_2O\ (g) \rightarrow 4H^+ + 4e^- + O_2 \tag{2}$$

$$\text{Cathode:} \quad 4H^+ + 4e^- \rightarrow 2H_2. \tag{3}$$

Routinely, the protonic ceramic cells are supported on Ni-based cermets, which are also selected to serve as the cathodes of the process due to their excellent hydrogen evolution electrocatalytic properties and incapability to tolerate the highly oxidizing environments of the anode. Hence, the critical part from an electrocatalytic point of view and primary challenge of H_2O electrolysis is the choice of the anodic electrocatalyst for the OER. Based on the required properties, the suitable materials should be triple ionic-electronic conductors (TIECs, H^+/O^{2-}, e^-) with catalytic activity for OER, adequate stability under steam and oxidizing atmospheres, as well as thermal expansion coefficient (TEC) values that close to the ceramic electrolyte under reaction conditions (temperature, humidity etc). So far, numerous materials have been investigated with different types of POs and misfit-layered oxides to have shown the optimum performance [36, 47–52]. It should be pointed out that protonic ceramic electrolytes typically are not pure proton conductors and, in many cases, electronic leakage affects the performance. Therefore, when referring to the efficiency and performance evaluation of the water splitting anodes, the faradaic efficiency (FE) to hydrogen generation should be also taken into consideration besides the current density and cell voltage. The steps for water reduction on composite electrodes can be seen in figure 2 and literature data are summarized in table 1.

4.1.1. OER electrocatalysts

The $BaCo_{0.4}Fe_{0.4}Zr_{0.1}Y_{0.1}0_{3-\delta}$ (BCFZY) was one of the first perovskites with high performance for H_2O splitting with FEs surpassing 90% at $\geqslant$1.0 A cm^{-2} and 600 °C under 20% H_2O. Meanwhile, BCFZY stability showed a low degradation rate (<30 mV/1000 h) after testing for up to 1200 h at 550 °C. The cell could even operate reversibly (i.e. both electrolysis and fuel cell) with considerable power-to-hydrogen efficiencies of up to 75% [48]. Besides BCFZY, the $PrNi_{0.5}Co_{0.5}O_{3-\delta}$ (PNC) perovskite displayed TIEC properties under similar conditions, particularly when a three dimensional structure was employed (figure 3(a)) [49]. The 3D PNC cell exhibited even higher current densities than BCFZY of ∼1.70 and 0.80 A cm^{-2} under the applied voltage of 1.4 V, at 600 °C and 500 °C, respectively, with good durability of 200 h at 500 °C in 10% steam concentration (figures 3(b) and (c)). Notably, important protonic currents were even observed at lower temperatures (0.55 A cm^{-2} at 450 °C and 1.4 V). The challenge for PNC is the important thermal conductivity coefficient (TEC) mismatch with BZCY-based electrolytes and doping of Fe has been shown to improve this issue, nonetheless, in expense of performance [80].

Double perovskites are another relevant class of materials with sometimes cases of superior performance to their single counterparts. $Ba_{1-x}Gd_{0.8}La_{0.2+x}Co_2O_{6-\delta}$ (BGLC) system was extensively investigated at the University of Oslo [45]. In order to fully utilize the role of oxygen vacancy in the lanthanide layer, BGLC should sustain the active double perovskite phase. This occurs when the x value is $\geqslant$0.5, otherwise, two-phases of BGLC and $BaCO_3$ may coexist [50]. Another highly active double perovskite proposed by the Haile's group is the $PrBa_{0.5}Sr_{0.5}Co_{1.5}Fe_{0.5}O_{5+\delta}$ (PBSCF) (figure 3(d)), that exhibited considerable water uptake capabilities [47]. The PBSCF, however, has a mismatch in TEC with the protonic electrolyte (23.7×10^{-6} PBSCF vs $9.5 \cdot 10^{-6}$ K^{-1} BZCYYb). To address this challenge the same group introduced a dense PBSCF layer of ∼100 nm thickness between the porous anode and the BZCYYb4411 electrolyte via

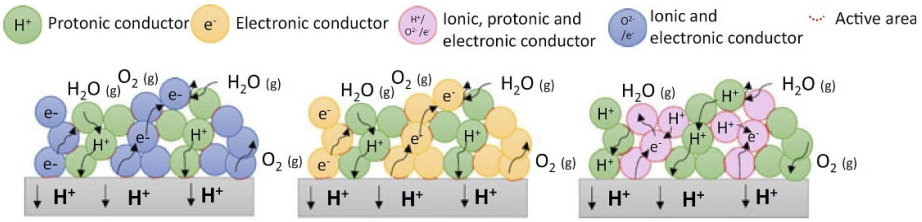

Figure 2. Electrochemical reaction steps for reduction of water on composite electrodes. Reproduced from [53], with permission from Springer Nature.

pulsed laser deposition (PLD) method, which improved the cell performance and decreased the cell resistance during electrolysis (figures 3(e) and (f)) [36].

More recently, misfit layered oxides based on $Ca_3Co_4O_{9-\delta}$ (CCO) with various dopings, such as $Gd_{0.3}Ca_{2.7}Co_4O_{9-\delta}$ (GCCO), and $Gd_{0.3}Ca_{2.7}Co_{3.82}Cu_{0.18}O_{9-\delta}$ (GCCCO) showed impressive performances, with almost the double the hydrogen production density compared to perovskites [51, 52]. Notably, this great performance was accompanied with a feeble degradation, even after 1400 h at 2.15 A cm^{-2} and 600 °C testing. The same group made further progress by proposing a basic Na-doped CCO (NCCO) as an OER electrode with even higher oxygen vacancy concentration over GCCCO due to the replacement of divalent Ca^{2+} by monovalent Na^{+} (figure 3(g)). XANES and XPS techniques validated that the valence of Co ion is increased by Na doping, resulting in more unpaired electron of Co, thereby promoting the absorption of oxygen intermediates and enhancing reaction kinetics. Moreover, such oxides displayed TEC values of $\sim 11.0 \cdot 10^{-6}\ K^{-1}$ which are close to BZCYYb electrolyte ($9.5 \cdot 10^{-6}\ K^{-1}$), partially eliminating the issue of thermal expansion mismatch (figure 3(h)) [51]. It worth mentioning that the current densities are the highest to being reported in the H_2O splitting process, surpassing 6.0 A cm^{-2} at 1.4 V and 600 °C (figure 3(i)), while the reversible operation could be sustained for >900 h [52].

4.2. CO_2 valorization to value-added chemicals or fuels

In the last decade, intermediate temperature (350 °C–600 °C) PCMRs have drawn significant interest for direct conversion of CO_2 into value-added chemicals by using H_2O or green H_2 as proton sources (figure 1) [54–57]. In the case steam is the hydrogen source, the reaction at the anode under external electrical potential is reaction (2) as shown above. In some cases, molecular H_2 may be the source of protons and the reaction at the anode is the reverse of reaction (3) (equation (4)). In both cases, protons are continuously transported to the cathode through the electrolyte, where they react with the CO_2 towards CO and CH_4, whereas H_2 can be formed through the side HER (equation (3)):

$$\text{Anode (oxygenelectrode)}:$$

$$H_2(g) + 2e^- \rightarrow 2H^+ \,(\text{molecular} H_2 \text{as reactant}) \tag{4}$$

$$\text{Cathode (Fuel electrode)}:$$

$$CO_2(g) + 2H^+ + 2e^- \rightarrow CO(g) + H_2O(g)\ \left(\Delta H_{298k} = \sim 41\ \text{kJ mol}^{-1}\right) \tag{5}$$

$$CO_2(g) + 8H^+ + 8e^- \rightarrow CH_4(g) + 2H_2O\ (g)\ \left(\Delta H_{298k} = \sim -165\ \text{kJ mol}^{-1}\right) \tag{6}$$

$$2CO_2(g) + 12H^+ + 12e^- \rightarrow C_2H_4(g) + 4H_2O(g)\ \left(\Delta H_{298k} = \sim -156\ \text{kJ mol}^{-1}\right) \tag{7}$$

$$mCO_2(g) + \left(H^+ + e^-\right) \rightarrow C_2 + xH_2O(g)\ (\Delta H_{298k} < 0). \tag{8}$$

According to the above cathodic reactions, the electrochemical conversion of CO_2 into syngas or hydrocarbons displays high complexity. It is obvious that the formation path of two-electron-transfer product (syngas) is simpler than the generation of multi-electron-transfer products, i.e., hydrocarbons. Moreover, the challenge of the latter process increases due to the requirement of lower reaction temperatures, and cathode materials that hinder hydrogen evolution in order to increase selectivity.

To this end, the operating conditions, e.g. temperature, reactant partial pressures, reactor design, and flowrates (affecting residence time over the catalyst) are expected to have a significant impact on the product distribution [15]. Specifically, by lowering the reaction temperature, the production of methane or hydrocarbons is favored to due to the exothermicity of the reactions involved, whereas an increase in temperature favors the endothermic reverse water–gas shift and steam methane reforming reactions, resulting in the formation of CO. This imposes a challenge in case the target is the production of hydrocarbons at temperatures in which PCMR exhibit significant proton conductivity (e.g. 600 °C). Even with high conductivity at lower temperatures (<600 °C), the kinetic factors should be also taken into

Table 1. Indicative recent literature in the most studied electrochemical processes in PCMRs.

a) Green hydrogen from steam

Working electrode (WE)	Protonic Electrolyte	Counter electrode (CE)	WE feed composition	T, °C	U_{cell}, V	j, A cm^{-2}	FE, %	Stability, h	References
BCFZY-BCZYYb7111	BCZYYb7111	Ni-BCZYYb7111	20% H_2O + 80% Air	600	∼1.6	1.38	98.6 (@0.4 A cm^{-2})	1200 (550 °C)	[48]
PNC*	BZCYYb4411	Ni-BZCYYb4411	10% H_2O + 90% Air	600	1.4	1.72	60–80 (15% H_2O)	—	[49]
				500		0.8		>200	
				450		0.55	—	—	
BGLC/BZCY72	BZCY72	Ni-BZCY72	1.5 bar H_2O (80 mbar O_2)	600	>1.6 V	˜0.28	80%–100%	>700 (0.0625 A cm^{-2})	[50]
PBSCF (PLD)*	BZCYYb4411	Ni-BZCYYb4411	Air (3% H_2O)	600	1.3	1.8	76	300 (550 °C, 1.3 V)	[36]
PBSCF						1.35	—	—	
GCCCO-BCZYYB7111	BCZYYb7111	Ni-BCZYYb7111	Air (20% H_2O)	600	1.3	2.15	>80%	1400 (2.15 A cm^{-2})	[51]
NCCO	BZCYYb1711	Ni-BZCYYb1711	20% H_2O, 80% Air	600	1.4	˜5.95	96.9 (@500 °C)	900 (FC and EC operation)	[52]

(Continued.)

Table 1. (Continued.)

b) Carbon dioxide valorization

Working electrode (WE)	Protonic Electrolyte	Counter electrode (CE)	WE feed composition	T, °C	j, A cm^{-2}	S_{CH4}, %	$S_{CO,}$ %	X_{CO2}, %	References
Porous Pt	BCZY27	Pr_2O_7-CeO_2/LSM/BCZY27	Ar (9% CO_2, 5% H_2)	700	<0.01	—	100%	17.8%	[54]
Ru-Co_3O_4/BZY (the ratio of Ru on Co_3O_4 is 2 wt%)	$BaZr_{0.85}Y_{0.15}O_3$ (BZY)	—	He (5% CO_2)	520–720	—	<40 H_2/CO_2 = <4 >90 H_2/CO_2 = 7	>60 reactants H_2/CO_2 ratio of 1 or 4) <10 (reactants H_2/CO_2 ratio of 7)	—	[55]
Ni/BCZYYb4411	BCZYYb4411	BCFZY-BCZYYb4411	N_2 (4% CO_2, with exhaust H_2 recycle)	450	−1000	∼85	—	∼85	[56]
			N_2 (4% CO_2)			∼62	—	∼55	
SFM-Ni0.175	BZCYYb1411	Ni-BCZYYb7111	Pure CO_2 (10 sccm)	400–600	50–300	—	97.1–99.8	—	[57]
CeO2/Ni-BZCYYb1711(the ratio of CeO_2 on cell is 3 wt%)	BZCYYb1711	PBSCF-BZCYYb1711	Ar (5% CO_2)	550	1250	17	20	—	[58]
Ni-BZCYYb1711						5	23		
Ca0.4/Ni-BZCYYb4411	BZCYYb1711	—	N_2 (CO_2)	300	—	87.49	—	57.86	[59]
Ni-BZCYYb4411						∼85	—	31.68	
Ni-BCZYYb7111 + a fixed bed of Ni/ CeO_2 at 300 °C	BCZYYb7111	BCFZY-BCZYYb7111	4.2% CO_2, 95.8% Ar	600	−2308	99.1	—	∼80	[48]
Ni-BCZYYb7111						7.1	—	∼38	
BZCY72-Ni	BZCY81	BZCY72-Ni	Ar (2% CO_2, 4% He)	450	—	99 (H_2/CO_2 ratio of 4)	∼ 0	86	[38]

(Continued.)

Table 1. (Continued.)

c) Methane activation

Reaction	Working electrode (WE)	Protonic Electrolyte	Counter electrode (CE)	T, °C	j, A cm^{-2}	U_{cell}, V	$X_{CH4,}$ %	$S_{prod.,}$ %	Stability, h	References
$CH_4 + 2H_2O \rightarrow CO_2 + 4H_2$	Ni-BZCY72	BZCY72	Cu	650	0.0113	2.4	80	∼95	24	[45]
$CH_4 + 2H_2O \rightarrow CO_2 + 4H_2$	Ni-BZCY	$BaZr_{0.8-x-y}Ce_xY_yO_{3-\delta}$	Ni-BZCY	800	4	∼0.46	∼100	98	2000	[60]
$CH_4 + 2H_2O \rightarrow CO_2 + 4H_2$	Ni-BZCY81	BZCY72	—	800	0.69	???	>99	—	1400	[33]
$CH_4 + CO_2 \rightarrow 2CO + 2H_2$	PBM-Ni_4Co-BZCYYb	BZCYYb	$NdBa_{0.75}Ca_{0.25}Co_2O_{5+\delta}$	700	4	∼0.5	>97	???	50	[61]
$CH_4 + CO_2 \rightarrow 2CO + 2H_2$	Ni-BZCY	BZCYYb	LSCF-BZCY/R-PCeCN	700	1.45	0.5	∼89	88	160	[62]
$6CH_4, \rightarrow C_6H_6 + 9H_2$	Cu + 6Mo/MCM-22 catalyst layer	BZCY72	Ni-BZCY72	700	0.040	???	∼11	>85	45	[34]
$6CH_4, \rightarrow C_6H_6 + 9H_2$	$BaFeMo_2O_{6-\delta}$	BCZY27	$BaFeMo_2O_{6-\delta}$	750	—	—	—	—	—	[63]
$6CH_4, \rightarrow C_6H_6 + 9H_2$	LSCM or LSM	BCZY27 + Pt	CeO_2	700	—	—	—	—	—	[64]

(Continued.)

Table 1. (Continued.)

d) Ethane and Propane dehydrogenation

Reaction	Working electrode (WE)	Protonic Electrolyte	Counter electrode (CE)	T, °C	U_{cell}, V	j, A cm^{-2}	Power (FC), mW cm^{-2}	$X_{alkane,}$ %	$S_{prod.}$,%	Stability, h	References
$C_2H_6 \rightarrow C_2H_4 + H_2$	Co–Fe-$(Pr_{0.4}Sr_{0.6})_3(Fe_{0.85}Mo_{0.15})_2O_7$	$BaCe_{0.7}Zr_{0.1}Y_{0.2}O_{3-\delta}$	LSCoF	750	1.005	0.66	348.8	∼50	>91	100	[65]
$C_3H_8 \rightarrow C_2H_4 + H_2/C_3H_6 + H_2$	$(Pr_{0.3}Sr_{0.7})_{0.9}Ni_{0.1}Ti_{0.9}O_3$/Ni-BZCY	BZCY	LSCF/BZCY	750	∼0.7	0.300	450	72	31 C_2 35 C_3 (650 °C)	50	[66]
$C_2H_6 \rightarrow C_2H_4 + H_2$	$(PrBa)_{0.95}(Fe_{0.9}Mo_{0.1})_2O_{5+\delta}$/Ni-BZCY	BZCY	$(PrBa)_{0.95}(Fe_{0.9}Mo_{0.1})_2O_{5+\delta}$	550		0.040		∼40	66.7	28	[67]

(Continued.)

Table 1. (Continued.)

e) Ammonia synthesis and decomposition

Reaction	Working electrode (WE)	Protonic Electrolyte	Counter electrode (CE)	T, °C	U_{cell}, V	j, A cm^{-2}	Rate of production	References
$N_2 + 3H_2 \rightarrow 2NH_3$	Pd	$SrCe_{0.95}Yb_{0.05}O3$ (SCY)	Pd	570	—	< 0.002	10^{-8} mol·s^{-1}	[68]
$N_2 + 3H_2 \rightarrow 2NH_3$	Ni–$BaZr_{0.7}Ce_{0.2}Y_{0.1}O_{2.9}$	BZCY72	porous Cu	620	2.4	~0.026	$4.1 \cdot 10^{-8}$ mol s^{-1} cm^{-2}	[69]
$N_2 + 3H_2 \rightarrow 2NH_3$	NiO-CeO_2	BCZYZ	Fe_2O_3	450	1.05	—	$4 \cdot 10^{-9}$ mol·s^{-1} cm^{-2}	[70]
$N_2 + 3H_2 \rightarrow 2NH_3$	Fe-K-NiO-BCZG	$BaCe_{0.7}Zr_{0.1}Gd_{0.2}O_{3-\delta}/Li_2CO_3$	NiO-BCZG	500	0.8	0.01	$1.87 \cdot 10^{-10}$ mol s^{-1} cm^{-2}	[71]
$CH_4, H_2O \rightarrow NH_3, CO_2, H_2$	VN-Fe	$BaZr_{0.8}Ce_{0.1}Y_{0.1}O_{3-\delta}$(BZCY81)	Ni-$BaZr_{0.7}Ce_{0.2}Y_{0.1}O_{3-\delta}$	600	0.63	???	68 mmol h^{-1} m^{-2}	[72]
$N_2 + 3H_2 \rightarrow 2NH_3$	Ni-BCZY	$BaCe_{0.2}Zr_{0.7}Y_{0.1}O_{3-\delta}$	Pt	500	2.75	0.080	26.8 nmol s^{-1} cm^{-2}	[73]
$2NH_3 \rightarrow N_2 + 3H_2$	Ru-LWO	$La_{5.5}WO_{11.25-\delta}$	Pt-LWO	350	1.2	2.5	231.1 μg h^{-1} cm^{-2}	[74]
$2NH_3 \rightarrow N_2 + 3H_2$	NiO-BZCY81	$BaZr_{0.8}Ce_{0.1}Y_{0.1}O_{3-\delta}$/ BZCY81	—	650	—	~0.7	—	[33]
$2NH_3 \rightarrow N_2 + 3H_2$	Ni/BZCY82	BZCY82	$BaCo_{0.4}Fe_{0.4}Zr_{0.1}Y_{0.1}O_{3-\delta}$ (BCFZY0.1)	600	—	0.9	—	[35]
$2NH_3 \rightleftarrows N_2 + 3H_2$	NiO-$BaCe_{0.7}Zr_{0.1}Y_{0.1}Yb_{0.1}O_{3-\delta}$	BCZYYbN		650	1.04	—	$1.2 \cdot 10^{-8}$ mol s^{-1} cm^{-2}	[75]
$2NH_3 \rightarrow N_2 + 3H_2$	Ni-Pd-BZCYYb	Pd-BZCYYb	$BaCo_{0.4}Fe_{0.4}Zr_{0.1}Y_{0.1}O_{3-\delta}$	650	0.6	1.25	—	[76]
$2NH_3 \rightarrow N_2 + 3H_2$	Fe-CeO_x/Ni-BzCYYb	BZCYYb	$PrBa_{0.5}Sr_{0.5}Co_{1.5}Fe_{0.5}O_{5+\delta}$	700	~0.4	1.8	—	[77]
$N_2 + 3H_2 \rightarrow 2NH_3$	$Sr_xTi_{0.6}Fe_{0.4}O_{3-\delta}$ ($x = 1$, 0.9)	BZCYYb	NiO/BZCYYb	650	0.6	0.0012 0.002	$6.84 \cdot 10^{-9}$ mol s^{-1} cm^{-2} ($x = 1$) $4.09 \cdot 10^{-9}$ mol·s^{-1}·cm^{-2} ($x = 0.9$)	[78]
$N_2 + 3H_2 \rightarrow 2NH_3$	$LaCu_{0.1}Fe_{0.9}O_{3-\delta}$/BZCYYb	BZCYYb	Ni/BZCYYb	650	0.4	—	$5.12 \cdot 10^{-9}$ mol·s^{-1}·cm^{-2}	[79]

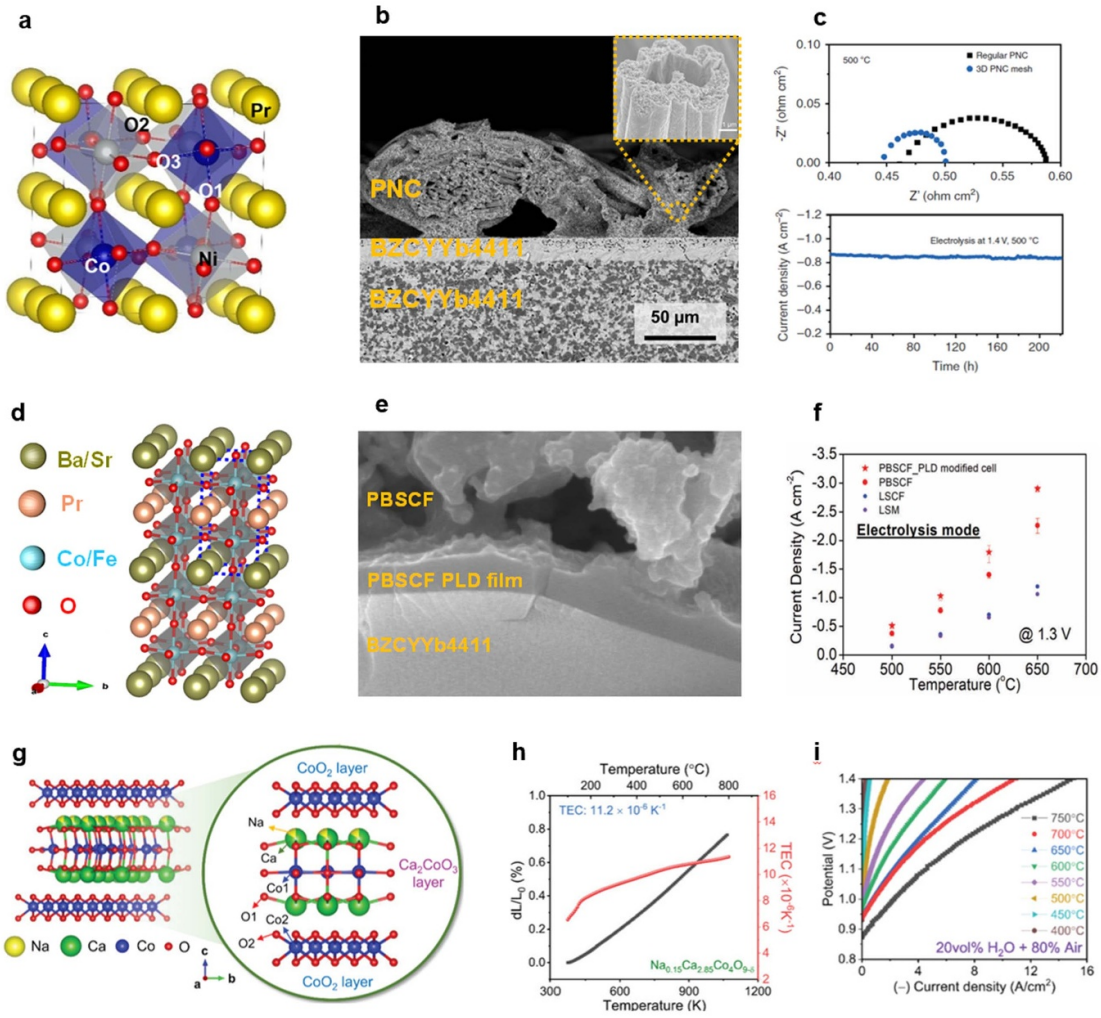

Figure 3. Important advances in OER electrocatalysts for hydrogen production from water splitting. (a) Crystal structure of the PNC perovskite, (b) SEM image of 3D structured PNC, (c) Impedance spectra revealing the enhancement due to 3D-stucture and stability. (a)–(c) Reproduced from [49]. CC BY 4.0. (d) Crystal structure of PBSCF double perovskite (e) SEM cross section image of the PLD PBSCF cell and (f) PBSCF with extra PLD layer benchmarking vs bare PBSCF, and standard air perovskite electrodes. (e) Reproduced from [47], with permission from Springer Nature. (f) Reproduced from [36] with permission from the Royal Society of Chemistry. (g) Crystal structure, (h) TEC and (i) IV polarization curves of NCCO. (g)–(i) [52] John Wiley & Sons. © 2022 Wiley-VCH GmbH.

account; HER dominates on metal surfaces, while on typical cathode-supported cells of Ni-BZCY, the reduction of CO_2 to CO is faster. Nevertheless, when the H_2/CO_2 ratio increases due to the higher current densities and thus, proton fluxes, the hydrocarbon formation is favored as shown by the stoichiometry of reactions (6)–(8).

It is therefore apparent that the selection of the cathodic electrocatalyst plays a decisive role in CO_2 conversion process. Extensive research has been devoted to developing new or modifying existing cathodic materials [54–59, 81–84]. For instance, by engineering the surface of CeO_2, Ye *et al* significantly enhanced CO_2 methanation [58], reaching CH_4 selectivity in the cell of 17%, but at production rate of only 0.19 ml min cm^{-2} at 550 °C. These values were further improved by Pan *et al* [56] where a higher CO_2 conversion and a CH_4 yield of 34.6% from CO_2 and H_2O as reactants were achieved at a current density of -1 A·cm^{-2} at 450 °C. The H_2-co-feed enhances CH_4 yield to 71.2% by utilizing H_2 that can be recycled in the reactor stream. The latter enhancement in the presence of gaseous hydrogen in the cathode atmospherew as partially attributed to electrochemical promotion of catalysis effect. Lastly, under fuel cell conditions (CH_4 fuel), a power density of 0.22 W cm^{-2} was reached at 550 °C.

Choi *et al* proved that surface $V_o^{\cdot\cdot}$ concentration of the catalysts was increased by tuning their surface basicity, which significantly decreases the CO_2 adsorption energy and promotes methanation [59]. The authors successfully synthesized a strong basic binary cathode of CaO-modified Ni-BZCYYb. Experimental evidence and DFT calculations (figures 4(a) and (b) suggested that CaO acts as an electron donor for the Ni-BZCYYb surface, thereby creating $V_o^{\cdot\cdot}$ on the BZCYYb surface through the reduction of Ce

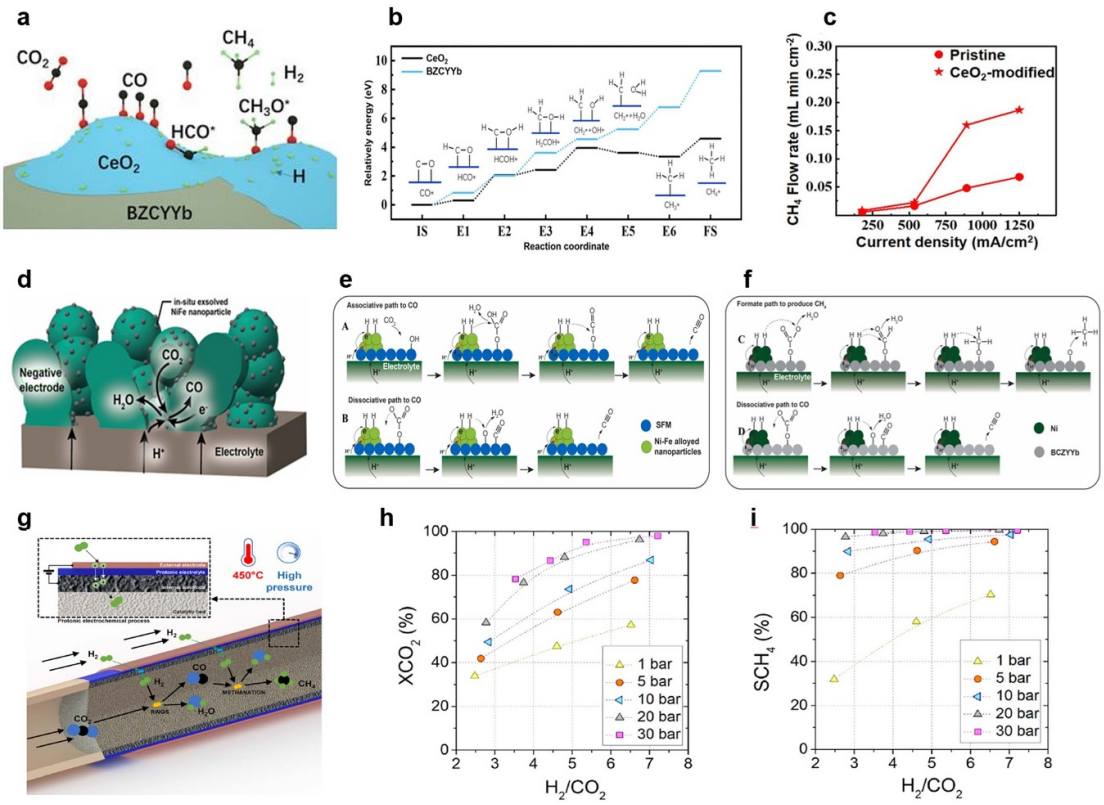

Figure 4. Indicative innovative concepts for CO_2 reduction. (a) CO_2 hydrogenation on the CeO_2-modified Ni-BZCYYb cathode surface. (b) Calculation of potential energy illustration for CO hydrogenation to CH_4 on BZCYYb and CeO_2. (c) Comparison of produced CH_4 with the pristine and CeO_2-modified cathode under different electrolysis currents. (a)–(c) Reproduced from [58] with permission from the Royal Society of Chemistry. (d) Schematic illustration of CO_2 reduction to CO in SFM-$Ni_{0.175}$ cathode-based cell. CO_2 reduction paths on the (e) SFM-Ni0,175 and (f) Ni-BZCYYb. (d)–(f) Reprinted from [57], Copyright (2022), with permission from Elsevier. (g) High pressure CO_2 methanation in a tubular PCMR. (h) CO_2 conversion rate and i. CH_4 selectivity as a function of pressure and H_2/CO_2 ratio at 450 °C. (g)–(i) Reprinted from [38], Copyright (2023), with permission from Elsevier.

($2Ce_{Ce}^{\times} + O_O^{\times} \rightarrow 2Ce_{Ce}' + V_O^{\cdot\cdot}$), which in turn decreases the activation energy for CO_2 adsorption. As a result, the CaO modification doubled the conversion compared to the bare Ni-BZCYYb (figure 4(c)).

An alternative for maximizing yield to methane was proposed by Duan *et al*, by connecting the exhaust of the PCMR with an external fixed bed reactor that enabled almost complete conversion of CO_2 to methane, 14-times higher than that of the single PCECs [48]. The same group also employed the *in-situ* exsolution NiFe nanoparticles from a SrFeMo-based double perovskite cathode. The bimetallic NiFe exsolution enabled higher CO_2 conversion to CO. The authors elucidated the difference between SFM-Ni and BZCYYb-Ni for selective CO_2 conversion by *in-situ* DRIFTS. The absorbed CO_2 on SFM-$Ni_{0.175}$ forms bicarbonate and monodentate carbonate, which were then reduced to CO, while on BZCYYb-Ni CO_2 was reduced to CH_4 and CO through formate path and the dissociative path of the monodentate carbonate, respectively [57]. An important development for CO_2 PCMRs was the recent report from Quina *et al* [38] in which a pressurized CO_2 reduction PCMR was demonstrated. The reaction was studied as a function of total pressure, temperature and H_2/CO_2 ratio resulting from the corresponding current density, reaching CH_4 yields of 99% with pressures above 20 bar. High pressure and a CO_2-rich atmosphere ameliorated the electrochemical behavior because of higher electrolyte hydration and boosted electrode kinetics [38].

4.3. Methane and biogas activation processes

As the main constituent of natural gas, methane (CH_4) is considered an ample and versatile energy source, both in terms of its use as a fuel (e.g. shipping) and commodity chemical transformations. Thus, methane can undergo transformations in a PCMR to yield syngas, aromatics and olefins. Steam reforming of methane (SRM) is today the dominant route for the production of syngas. In 2016, Kyriakou *et al* [45] demonstrated low temperature (450 °C–650 °C) SRM by employing a Ni-BZCY72/BZCY72/Cu PCMR. The protons removal allowed the methane conversion to surpass 80% at 600 °C, which cannot be achieved in a conventional catalytic reactor operating at the same conditions of pressure and temperature. Moreover, the continuous hydrogen recovery and the decrease in operation temperature favored the water gas-shift

reaction, and therefore, the selectivity towards CO_2 (∼99%). Malerød–Fjeld *et al* [60] carried out SRM by using the same tubular reactor, albeit in a Ni-BZCY symmetrical configuration. Full methane conversion was achieved at 800 °C by continuously removing hydrogen, reaching impressive current densities of 4 A cm^{-2}. More recently, Clark *et al* [33] expanded this concept of hydrogen extraction to processes beyond SRM, such as biogas and ammonia whilst, developing a pioneering PCMR stacked module. The stack formulation enables up to 400 A of total current, H_2 production of up to 0.34 kg d^{-1} from methane, 0.31 kg d^{-1} from biogas, and 0.34 kg d^{-1} from ammonia.

Dry reforming of biogas (CH_4, CO_2) is another intriguing route for generating syngas, aiming to enhance and consolidate global decarbonization protocols. Hua *et al* [61] reported on an electrochemical reactor with a Ni_4Co bimetallic catalyst on $PrBaMn_2O_{5+\delta}$ (PBM)-BZCYYb composite anode. Notably, the authors showed electrochemical stability in a 50 ppm H_2S-containing CH_4/CO_2 mixture at a current density of 1 A·cm^2 with up to 0.8 W cm^{-2}. Wang *et al* [62] employed anode-supported cells and reported R_p of ∼0.15 Ω and R_Ω of ∼0.17 Ω at 700 °C, whereas the peak power densities reached 0.697 (with reforming layer) and 0.662 W cm^{-2} (without layer), indicating that the presence of the reforming layer does not contribute significantly to the performance improvement despite its catalytic properties.

One of the first examples of methane conversion to hydrocarbons was the simultaneous production of C_2 hydrocarbons and H_2 or electricity in a PCMR (upper case of figure 1(b)) [85]. By employing an Ag cathode and LSCoF at temperatures between 700 °C–850 °C and atmospheric pressure, low power densities of <1.2 mW cm^{-2} were achieved due to the ohmic resistance of the high thickness (2 mm) $SrZr_{0.9}Y_{0.1}O_3$ electrolyte supported cell. Interestingly, the continuous hydrogen pumping from methane in fuel cell mode resulted in an up-to 20% increase in C_2's reaction rate compared to the open circuit operation. The overall cell reactions for ethylene as primary product are described by the following equations:

$$\text{Electrolysis mode}: 2CH_4 \rightarrow 2H_2 + C_2H_4 \quad (9)$$

$$\text{Fuel cell mode}: 2CH_4 + O_2 \rightarrow C_2H_4 + 2H_2O. \quad (10)$$

In 2016, Morejudo *et al* [34] reported on the direct conversion of methane to benzene (C_6H_6) using a $BaZrO_3$-based hybrid catalytic-electrochemical membrane reactor of tubular configuration that pumps hydrogen and supplies small amounts of oxygen (co-ionic) to avoid coking, leading to increased catalyst stability (figure 5). Up to 80% carbon efficiencies were reached, aiding to the process viability. Nonoxidative dehydrogenation of ethane (NDE) to wards ethylene in the presence of nitrous oxide has been realized in a PCMR bearing a supported $BaZr_{0.1}Ce_{0.7}Y_{0.1}Yb_{0.1}O_{3-\delta}$ membrane, where the cogeneration of electricity and ethylene was achieved by using a PSFNCu ($Pr_{0.6}Sr_{0.4}Fe_{0.8}Nb_{0.1}Cu_{0.1}O_{3-\delta}$) PO catalytic layer in the anode [86]:

$$C_2H_6 + N_2O \rightarrow C_2H_4 + N_2 + H_2O \quad (11)$$

High performance in NDE was attributed to the stability of the perovskite during reduction and oxygen vacancies. The maximum power density was 200 mW cm^{-2} (750 °C), while an ethane conversion of ∼45% and selectivity for ethylene of ∼93% were obtained. Incorporation of nitrous oxide conversion resulted in a 208 mW cm^{-2} (750 °C) power density, 45.2% ethane conversion, 92.5% ethylene selectivity, and 19% conversion for N_2O, successfully demonstrating the simultaneous conversion of greenhouse gas N_2O and olefin production. A different cell reactor with a double $Ba_2FeMoO_{6-\delta}$ (BFMO) perovskite [63] was also reported for the promotion of methane dehydroaromatization (MDA) reaction in a symmetrical cell configuration. BFMO exhibited adequate compatibility with BCZY27 stability for a prolonged period under reducing conditions (5% H_2) and stability in 10% CH_4 at 750 °C. The optimized ASR of the electrode reached 6.8 Ω cm^{-2} at 750 °C in a humid H_2 atmosphere. More recently, Almar *et al* [64] investigated various perovskite electrode formulations, coupled with BCZY27 electrolyte where the infiltration of Pt/CeO_2 decreased R_p to 0.7 Ω cm^{-2} at 700 °C in a reducing CH_4 atmosphere. MDA at 700 °C has also been investigated using a U-shaped ceramic hollow $La_{5.5}W_{0.6}Mo_{0.4}O_{11.25-\delta}$ (LWM0.4) fiber membrane reactor with a zeolite-based catalyst (Mo/HZSM-5) [87]. Removal of H_2 was employed to overcome thermodynamic limitations to increase methane conversion and aromatics yield with the latter reaching 70%. Coking was observed due to the removal of hydrogen but regeneration afforded the recovered catalyst.

4.4. Ethane and propane dehydrogenation

Ethylene and propylene are amongst the most important compounds in chemical industry due to their use as building blocks, particularly for polymers. The combination of the PCMRs with ethane or propane dehydrogenation towards lower olefins has significant advantages. In electrolytic operation, the hydrogen is

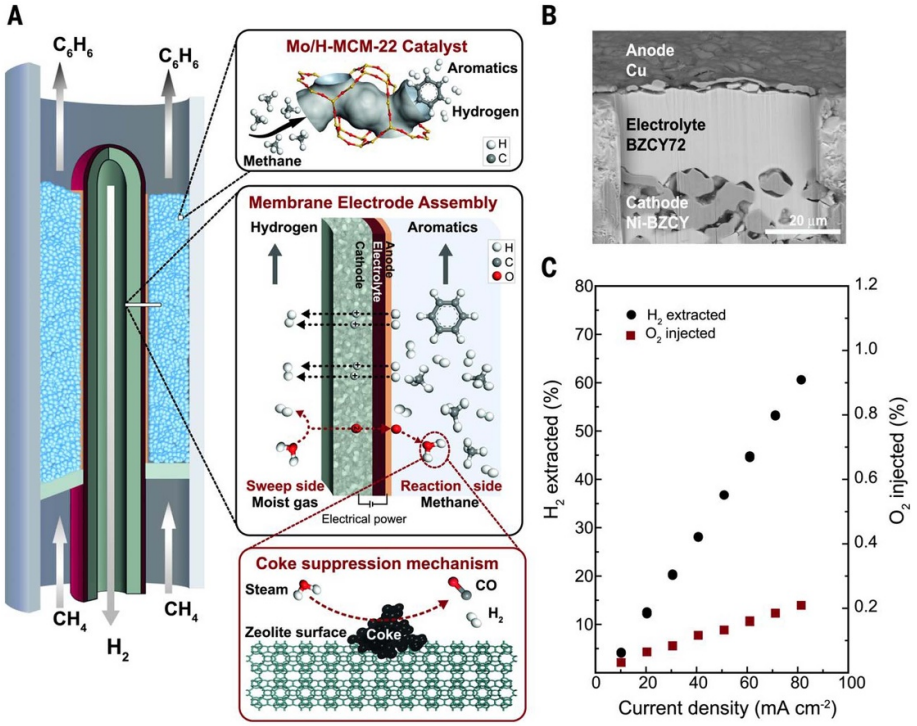

Figure 5. Current controlled co-ionic membrane reactor. (a) Conversion of methane to aromatics. (b) SEM images of the assembly. (c). H_2 extraction and O_2 injection vs current density at 700 °C. From [34]. Reprinted with permission from AAAS.

directly separated from the dehydrogenation chamber (anode), by simultaneously shifting the equilibrium to the desired olefins and hydrogen products. Moreover, by introducing air at the cathode, the overall cell reaction becomes a partial oxidation which is spontaneous, thus offering the chance for the cogeneration of ethylene and power.

One of the first efforts to exemplify this concept was the work of Liu *et al* [65] by employing a double-layer PO $(Pr_{0,4}Sr_{0.6})_3(Fe_{0.85}Mo_{0.15})_2O_7$ (PSFM) with bimetallic exsolution of Co–Fe nanoparticles deposited over a BZCY electrolyte. The authors reported high power densities of ∼0.45 W cm^{-2} in ethane at 750 °C, with ethylene selectivity >91% and cogeneration of electricity. By elevating the temperature, the ethylene yield was improved but with lower selectivity due to coking. In 2020, Shi *et al* [66] reported on the generation of ethylene and propylene in using propane as feedstock. $(Pr_{0.3}Sr_{0.7})_{0.9}Ni_{0.1}Ti_{0.9}O_3$ was employed as a catalytic anode-supported layer with exsolved Ni-nanoparticles. BZCY was employed as an electrolyte, with an LSCF-BZCY cathode. In a 9:1 propane—water mixture tolerance against coking was observed, suggested to occur due to the increased activity of the catalytic layer. At 700 °C, the conversion to propylene reached 36% and to ethylene 32%, at a current density of 300 mA cm^{-2}. Similarly, several groups have demonstrated cogeneration of ethylene and hydrogen at elevated temperatures by changing the anodic perovskites and protonic ceramic electrolytes, achieving yields of up to 40%, but with rather low power densities for upscaling.

On the other hand, Wu *et al* [67] proposed a planar PCMR which operates at considerably lower temperatures to achieve ethane dehydrogenation (∼550 °C). Alkane dehydrogenation is even more challenging at lower temperatures and therefore, the electrochemical cell reactor consisted of a highly active PtGa-ZSM-5 catalyst over a porous $(PrBa)_{0.95}(Fe_{0.9}Mo_{0.1})_2O_{5+\delta}$ anode in a Ni-BZCYYb-based cell. The authors reported an <40% ethane conversion with an ethylene yield of up to 26.7%, however, at low current densities (40 mA cm^{-2}) due to the low temperatures employed.

4.5. Ammonia synthesis and decomposition

4.5.1. Dinitrogen fixation

Ammonia synthesis from its constituent elements was always considered a holy grail for modern chemistry and engineering due to the ability of ammonia to act as hydrogen energy carrier or be further utilized in fertilizer synthesis [88]. Ammonia synthesis at atmospheric pressure in PCMRs was first reported by Marnellos and Stoukides [68] in 1998 where an Pd on SrCeYb was used to exemplify the concept while several works that followed have verified its feasibility but with poor faradaic efficiencies. More recently, Vasileiou *et al* [89] made an effort to enhance the open-circuit (catalytic) rate of a catalytically active

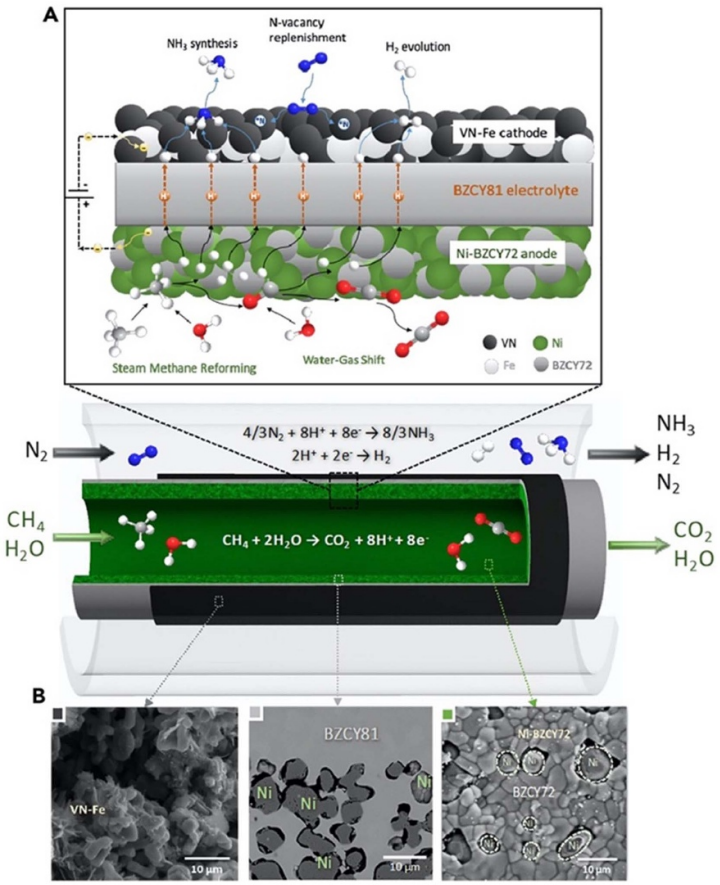

Figure 6. Integration of hydrogen production, purification, and ammonia synthesis in the PCMR. (A) At the Ni-BZCY72 anode compartment, (conversion of CH_4-H_2O mixture to CO_2 and H^+, the latter transported to the VN–Fe cathode. On VN, lattice N reacts with H^+ to form NH_3, while the N-vacancy is replenished by dissociated N_2 from the gas-phase. (B) SEM images of VN–Fe cathode surface, cell cross-section, and Ni-BZCY72 anode surface after exposure to 20% H_2/N_2 at 650 °C for 48 h. Reprinted from [72], Copyright (2020), with permission from Elsevier.

Ni-BCZY (Electrochemical Promotion of Catalysis, EPOC, study). The net electrocatalytic rate (difference between closed- and open circuit rate) was found ∼1.5 g h^{-1} m^{-2}, with faradaic efficiencies surpassing 6%. The same group used the same cell but in a double chamber configuration in order to control the co-fed hydrogen [69]. Without gaseous H_2 addition, at 620 °C the highest ammonia production rate was ∼0.5 g h^{-1} m^{-2}. However, by co-feeding N_2 and H_2 a net electrocatalytic rate of 2.4 g h^{-1} m^{-2} was reported, translating to a >140% enhancement compared to the OCV (catalytic) rate.

Klinsrisuk and Irvine [70] examined the same reaction with a different electrolyte membrane, namely $BaCe_{0.5}Zr_{0.3}Y_{0.16}Zn_{0.04}O_{3-\delta}$ (BCZYZ). The anode was NiO/CeO_2 and the cathode was a PdO-impregnated iron oxide while no hydrogen was co-fed. The electrocatalytic ammonia production rates reached ∼3 g h^{-1} m^{-2} at 450 °C, but again with very low FEs (<2.5%). Through a different doping strategy, Lei *et al* [71] used a $BaCe_{0.7}Zr_{0.1}Gd_{0.2}O_{3-\delta}$ (BCZG) electrolyte with Li doping which enhanced ionic conductivity and acted as a co-sintering aid. Ammonia synthesis was then realized in a cell with Fe- and K-doped Ni-BCZG and Ni-BCZG electrodes. At 500 °C, a formation rate of ∼0.1 g h^{-1} m^{-2} was achieved, with a current efficiency of 0.53% at 0.8 V.

With the brisk developments in tubular protonic electrolytes, Kyriakou *et al* [72] utilized a tubular barium zirconate PCMR to demonstrate the integration of all key steps of an ammonia plant, i.e. hydrogen production/purification from methane steam reforming and water gas shift, as well as ammonia synthesis, in a single PCMR (figure 6). By introducing for the first time the nitride electrodes high temperature electrochemical cells (VN–Fe) an up to 14% FE was achieved at low applied voltages for dinitrogen reduction (<0.8 V) due to the use of the Mars-van Krevelen mechanism. Practically, lattice nitrogen from the nitride reacts with protons and the vacancy in the nitride is replenished by the dissociation of the gas phase dinitrogen. The system also made use of the capability of the PCMR to shift the equilibrium of hydrogen production through its *in-situ* extraction from the Ni-BZCY anode, thus delivering almost pure CO_2 for easier capture and further use.

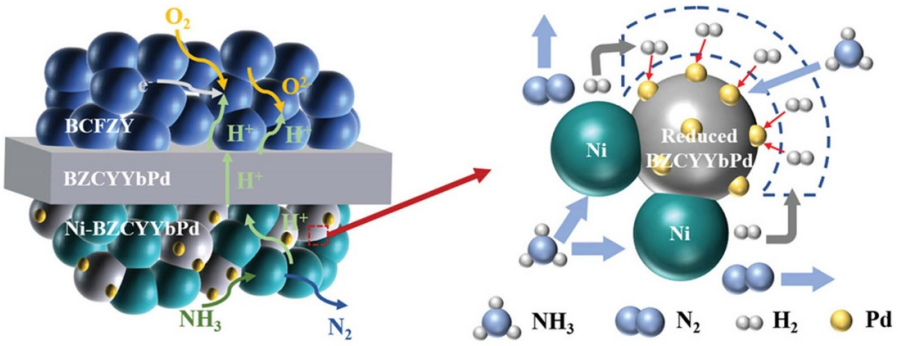

Figure 7. Pd-doped BZCYYb perovskite oxide, namely $Ba(Zr_{0.1}Ce_{0.7}Y_{0.1}Yb_{0.1})_{0.95}Pd_{0.05}O_{3-\delta}$ that functions as electrolyte and anode. [76] John Wiley & Sons.© 2021 Wiley-VCH GmbH.

Another intriguing strategy to enhance the FE to ammonia in a similar PCMR was shown by Sharma *et al* [73], where protons from water oxidation reacts with the plasma-activated nitrogen molecules to yield ammonia. Ammonia production rate reached 16.4 g h^{-1} m^{-2} accompanied with an up to 88% FE at 500 °C. In order to decrease the temperature and slow down ammonia decomposition kinetics, a PCMR with a $La_{5.5}WO_{11.25-\delta}$ (LWO) membrane, a Pt@LWO anode and Ru@LWO cathode, operating at 350 °C, was fabricated by Weng *et al* [74]. A high FE of 43.8% was reported, with ammonia production rate of 2.3 g h^{-1} m^{-2} at a current density of 2.5 mA cm^{-2}. This reactor also displayed durability after 100 h under N_2 reducing conditions.

4.5.2. Hydrogen recovery from ammonia

The Ni-BZCY (or Yb) electrodes have shown excellent capability in decomposing ammonia to its elements, thus rendering anode-supported proton conducting cells suitable for ammonia fuel cell operation [33]. Nevertheless, besides the demonstration by Duan *et al* [35] and the work of Clark *et al* [33] discussed above, most of the research reported on anode functionalization with different active metals to achieve even higher performances. A reversible PCFC was reported by Zhu *et al* [75], comprising of a Ru-$(BaO)_2(CaO)(Al_2O_3)$ ammonia catalyst. A maximum power output of 944 mW cm^{-2} was achieved at 650 °C using NH_3 fuel (877 mW cm^{-2} for H_2 fuel at the same temperature). At 600 °C, stability was displayed for 1250 h. He *et al* [76] reported a Pd-doped BZCYYb PO, namely $Ba(Zr_{0.1}Ce_{0.7}Y_{0.1}Yb_{0.1})_{0.95}Pd_{0.05}O_{3-\delta}$ that functions as electrolyte and anode. Exsolution of Pd was observed, and a superior proton conductivity compared to BZCYYb. The Ni-PdBZCYYb composite anode reached a power density of ∼0.75 W cm^{-2} at 650 °C with ammonia fuel. Importantly, the exsolved Pd metal sites were reported to protect Ni-particles against ammonia attack. Stability was exhibited for 350 h in H_2 and NH_3 atmospheres at 550 °C (figure 7). Hou *et al* [77], added an iron-doped ceria catalyst layer on Ni-BZCYYb anode cermet achieving 1.06 W cm^{-2} at 700 °C due to the Fe-Ce catalyst inhibiting iron nitride formation (iron poisoning).

4.6. Opportunities, directions and possible dead ends

Electrification of industrial processes towards high-value chemicals or fuels by utilizing renewable sources is critical if carbon neutrality is to be achieved in the coming years. Concurrently, the direct use of hydrogen as a feedstock or product is of crucial importance for the chemical industry and in extend for our society since it diminishes the CO_2 emissions and hence, its production technology is going to have a considerable impact on energy economy. To this direction, PCMRs may be utilized not only as electrochemical reactors but also as *in-situ* separators, thus offering high energy efficiencies and flexibility to several processes of industrial interest. This is due to the integrated approach of a solid ionic membrane with a catalytic reactor that also display unique features; (a) process intensification and thus, higher efficiency through the channeling of the heat released by an exothermic reaction at one of the electrodes or the ion transport (joule effect) through the electrolyte to an endothermic reaction at the counter side (e.g. ammonia synthesis and steam methane reforming or steam electrolysis). (b) Shift of the equilibrium of the reaction for maximizing the product yield while purifying or storing hydrogen. The different processes described in the previous section of the present article clearly exemplify the applicability and the potential of the PCMR systems in processes varying from energy to environmental remediation. Below, we explore some possible directions and challenges for different processes, as well as new opportunities on unidentified or immature systems.

4.6.1. Near-term targets: SoA PCMR components and upscaling for H_2 generation

An impressive aspect is the considerable progress that has taken place in the last decade in design and fabrication of cells of both tubular and planar configurations. The two designs have their origins from the traditional oxide ion-based cells. Planar design has the advantage of lower cell reactor sizes and better current collection whereas, the tubular geometry transcends in terms of thermomechanical properties (e.g. during pressurization for H_2 recovery) and heat transfer distribution [90]. In addition to this, the choice of the geometry in PCMR can be even more significant due to the wider range of products and the sensitive balance between them in order to obtain the highest selectivity (or FE) to the desired product. The leading role in manufacturing tubular ceramic proton conducting cells has CoorsTek Membrane Sciences AS that develops a high Zr content membrane with an electrolyte thickness of 25–30 μm. The BZCY electrolyte film is supported on a porous Ni-BZCY cermet, which, at the same time, serves as an electrode [28]. The cell allows high H^+ fluxes (on the order of μmol H_2 s^{-1} cm^{-2}), exhibits appreciable mechanical and chemical stability and has thus been successfully used in several cases of H_2O splitting, CO_2 valorization and hydrogen recovery at low temperatures and high pressure [33]. These cells have significantly contributed in advancing the PCMR technology as essentially meet the requirements for H^+ flux and stability to a certain extent. On the other hand, planar cells have been mainly demonstrated for PCMR applications only as button cells of a few cm^2 size, whilst the scaling has been carried out in some decades of cm^2 only in fuel cell operation. Thus, further experimental validation is necessary for evaluating their performance during water electrolysis and subsequently, as PCMRs for more complex reaction schemes [27, 91, 92].

The above-described progress in membrane materials and design in combination with an urge in the development of Power-2-X technologies for electrical power storage imply a momentum for larger scale demonstration projects to explore the potential of protonic cells. For instance, the extensively investigated reversible H_2/H_2O SOECs could lead the way for demonstration of the same concept in PCMRs but issues related to decreased FE due to electronic leakage should be addressed prior to this. Outstanding current densities have been achieved with several anodic electrodes such as PBSCF and more recently NCCO ($\sim$5–6 A cm^{-2} at 600 °C and around 2–3 A cm^{-2} at 500 °C) that exceed commercialization targets, albeit their long-term stability is debatable. An interesting approach to be considered here is the operation of the cell in reversible mode (practically creating a hydrogen flow battery) to enhance their flexibility and possibly lifetime. The latter has been exemplified in oxide ion cells where the partial operation in fuel cell mode instead of continuous electrolysis revealed 'healing' properties [14].

Unquestionably, one of the most promising approaches for PCMR upscaling is the recovery of pressurized hydrogen from biogas, methane or ammonia feedstocks, as proposed by Clark *et al* in a tubular geometry configuration (figure 8) [33]. The authors presented a unique stack with 36 cells (584 cm^2, 400 A in total) of total active area with a novel interconnect material that achieves complete conversion of the feedstocks as well as >99% recovery to pressurized hydrogen of up to 140 bar when ammonia was employed. This PCMR approach is benefited by the high hydrogen concentrations produced even when no current or voltage is imposed (open-circuit conditions). For instance, ammonia decomposition takes place spontaneously at high temperatures over an effective catalyst (as Ni-BZCY) which in turn benefits the FE since hydrogen oxidation to protons is much simpler compared to OER (i.e. H_2O splitting). Additionally, proton pumping shifts the equilibrium to the desired hydrogen production side during the separation (process intensification), while high efficiency can be achieved due to channeling of heat to the endothermic anodic reactions through the joule effect. The system reported by CoorsTek currently generates $\sim$0.5 kg d^{-1} of hydrogen and it could be the bellwether system for navigating the developments of upscaling projects, hence validating the potential for commercial viability of the PCMR's in the coming years.

4.6.2. Long-term targets: chemicals and fuels beyond hydrogen

The production of hydrocarbons from the conversion of carbon dioxide or alkanes displays another attractive direction towards chemical energy storage as evident from the extensive number of reported works on electrocatalytic and membrane materials, as well as alternative concepts. Co-electrolysis of CO_2 and H_2O is an aspect shown by Irvine's group more than a decade ago, followed by the ground-breaking developments in membranes and positrodes by O'Hayre's and Haile's groups. The main product under the operating conditions was syngas while methane was produced at minor concentrations below 500 °C due to thermodynamic and kinetic limitations, i.e. low H/C ratios due to the decreased proton flux. This challenge was addressed by O'Hayre's group through the downstream catalytic methanation of the produced syngas at 300 °C in order to achieve higher methane yields [35].

The single-step approach can be rather beneficial and it came through the development of high performance and pressurizable proton conducting membranes that enabled appreciable proton flux below 500 °C by simultaneously creating favorable thermodynamics for direct methanation. It should be noted, however, that complete conversion of CO_2 to CH_4 is achieved through low flowrates ($\sim$3 ml min^{-1} of CO_2)

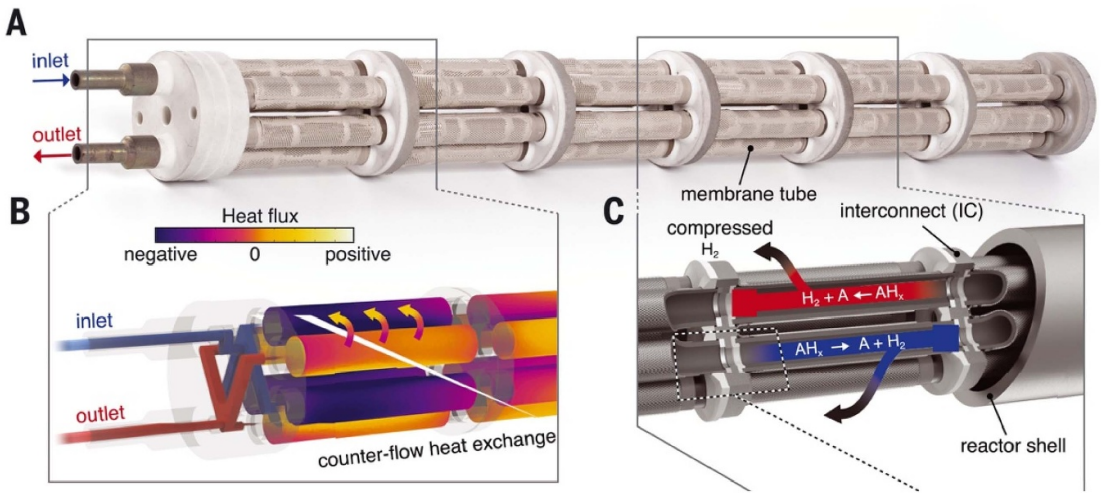

Figure 8. PCMR stack for industrial H2 production. (a) The proposed PCMR configuration for upscaling (height:43 cm, diameter: 4 cm). (b) Microthermal heat integration with outward heat flux from the cells. (c) U-bend type of gas flow of the generic molecule AH_x. From [33]. Adapted with permission from AAAS.

and thus, low space velocities when considering the weight of the Ni-based electrode, while hydrogen feedstock was used instead of steam. To address the former issue, a combination of the above approaches would be beneficial by introducing a heterogeneous catalyst bed in the PCMR, in a similar manner to what has been shown previously in ceramic electrolyte membrane reactors for methane activation [34, 75, 93, 94]. By introducing a catalyst bed, hydrogen is evolved over Ni cermet and subsequently it reacts with the carbon-containing molecule over the catalyst bed, circumventing the need for reinventing the MEA. A similar approach can also aid other systems of equilibrium reactions with decreased product volume favored by pressurization, such as ammonia synthesis and possibly higher hydrocarbon formation from CO/CO_2 mixtures. In addition, for the ideal case where H_2O is the hydrogen feedstock, efficient and stable OER electrocatalysts exhibiting high performance (>0.5 A cm^{-2}) close to 400 °C–450 °C, such as the calcium-cobalt misfit layered, and the double perovskites discussed in the steam electrolysis section may answer these challenges.

Dehydrogenation of ethane or methane to C_2s is a concept is of crucial importance due to the wide use of ethylene in the production of polymers. The interesting aspect is that the reaction of an alkane towards alkenes (e.g. ethane to ethylene) constitutes a partial oxidation reaction when air is fed to the cathode, and thus, creates a significant electromotive force (>0.9 V at 700 °C) for the cogeneration of power. Of course, the alternative could have as target the production and in-situ recovery of hydrogen when no air is supplied to the cathode. The idea of chemical cogeneration [13] of electrical power is a rather intriguing aspect of EMRs. The concept was first proposed by Vayenas [95], while later it was applied by several research groups. Nevertheless, when dealing with dry hydrocarbon systems, the major issue is coking. So far, several pioneering works have proposed solutions with stable perovskite anodes during ethane dehydrogenation to ethylene with high yields and selectivities, while maintaining adequate stability for >100 h.

SOEC systems commonly operate with gas reactants and products due to the high temperatures involved. There are of course some special cases such as the direct carbon (solid or in molten carbonates) fuel cells with different coals as feedstock, but such approaches with fossil fuels cannot be considered anymore sustainable. The substitution of coal with solid biomass could tackle these issues, but the high gasification rates of biomass at temperatures above >500 °C due to the high content of volatile matter, imposes complexity and thus, critical engineering challenges for gas recirculation towards the exploitation of the overall energy content of the fuel feedstock. To this direction, the SoA PCMRs could open new horizons for the direct utilization of bio-based solid feedstocks as has been shown by Kyriakou *et al* [45]. In this work [96], a tubular Ni-BZCY configuration was proposed to achieve hydrogen production and recovery from steam gasification of carbon black (99% pure carbon at 600 °C and atmospheric pressure. An alternative would be the swap of the feedstock to biomass (e.g. biochars) or waste, in order to take advantage of the temperature compatibility of the gasification process and high protonic membrane flux towards in situ hydrogen recovery (or pressurization as well), pure CO_2 for CCUS by exploiting the overall heat content of a low-cost renewable source or waste.

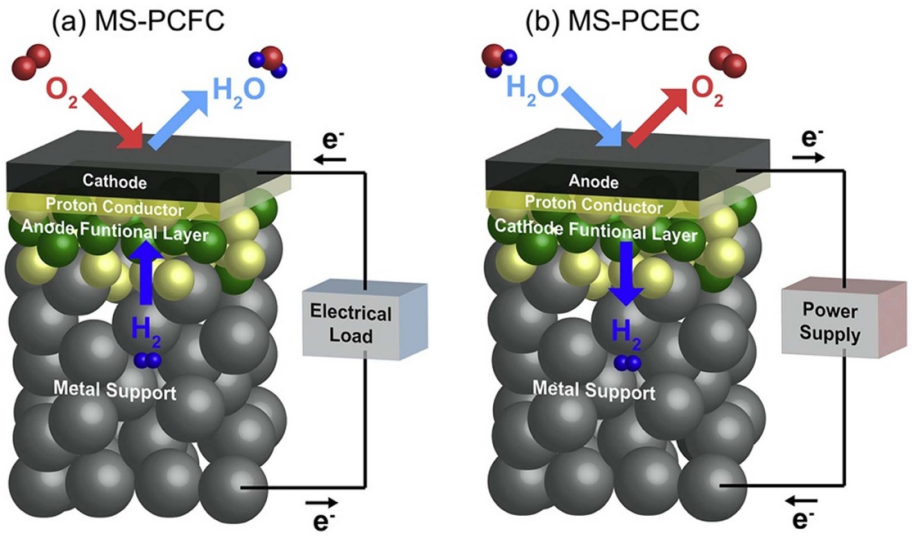

Figure 9. Schematic representation of the cell structure. (a) Metal-supported PCFC, (b) metal-supported PCEC. Reprinted from [97], Copyright (2019), with permission from Elsevier.

4.6.3. Circumventing dead ends with new strategies

A wider deployment of the PCMRs in the coming years will put forward several applications related to direct electrified synthesis. Various reaction schemes may integrate highly complex processes with electrode properties beyond Ni-BZCY will necessitate the reinvention of the membrane-electrode assembly and its design. For instance, the ammonia synthesis from steam and nitrogen will require the development of Ni cermet-free electrodes since the current Ni cermets favor the side HER when used as cathodes or are oxidized when used as anodes for OER. Therefore, this will require new PCMR configurations as shown in figure 9, with cells beyond electrode-support through, for instance, the introduction of an independent porous backbone to act as support for the new MEA [97]. Other examples for the need of new designs is related to the production of hydrocarbons from CO or CO_2 due to the simultaneous production of steam that limits the system and increase its complexity. The use of co-ionic membranes that consist of protonic ceramic and oxygen ion conducting could increase the utilization of the current (i.e. better FE) since the H_2O produced can be concurrently electrolyzed in the same electrode, and thus, the present systems should be re-engineered. The preparation of the electrolyte in this case would be challenging, however, Ivanova *et al* [98] proposed a solution by constructing a $BaCe_{0.8}Eu_{0.2}O_{3-\delta}$:$Ce_{0.8}Y_{0.2}O_{2-\delta}$ dual phase electrolyte.

Dinitrogen fixation is by far the most challenging electrochemical reaction that has been studied in PCMRs. To carry out this reaction at higher temperatures offers a unique advantage due to the enhanced kinetics for the endothermic cleavage of the dinitrogen triple bond. In addition, the demonstration of metal nitrides (or oxynitrides) as electrocatalysts could offer a new alternative in the field of electrocatalytic research. Advanced modeling studies and experimentation should be combined towards understanding the underlying cathode processes at nanoscale in order to demonstrate significantly improved faradaic efficiencies and reaction rates to ammonia. Certainly, the targets for the process regarding feasibility as set by Giddey *et al* about a decade ago, and confirmed by the DoE in US, cannot be reached in a blink of an eye. There is, however, an urgency for a drastic increase in the reported rates and faradaic efficiencies that would offer some boost to the technology. For instance, expanding DFT modeling to prediction of new electrocatalysts beyond liquid electrolyte systems [99], dedicated to higher temperatures whereby PCMR operate could be a solution. Other alternatives could be the increase in the reactor pressure to suppress HER [38] or the hybrid plasma-PCMR approach proposed by Sharma *et al*, in which FEs up to 88% were reported. For the latter of course, some detailed energetic analysis should be performed in order to elucidate the actual energy efficiency of this hybrid system.

Finally, ammonia production with high FEs can be also expected when the nitrogen source is not atmospheric dinitrogen, as for instance in NO_x reduction. In this case, the nitrogen already exists in its atomic form, thus eliminating the challenging dinitrogen triple bond cleavage and rendering its hydrogenation much simpler. A similar approach has been successfully demonstrated in low temperature electrochemical systems with nitrate source with promising results [100]. Although very attractive, this route should be not considered as a direct alternative to technologies utilizing the abundant atmospheric dinitrogen, such as the HB process and the electrocatalytic dinitrogen fixation, since NO_x feedstock is not

equally abundant. Nonetheless, it would be interesting to explore this reaction scheme in PCMRs by starting from the evaluation of electrocatalytic activity and stability of the SoA Ni cermets in the presence of the oxidizing NO_x species.

5. Conclusions

PCMRs constitute an exciting platform for electrification processes with high potential in terms of efficiency and flexibility. During the last few years, significant progress has not only been made on the cell components, but also on increasing the readiness level through scaling project demonstration. Among the explored technologies, the production of pressurized hydrogen from sustainable sources, such as biogas and ammonia, seems to be closer to commercialization, while significant steps forward have been made in the generation of green hydrogen from steam electrolysis. Other processes, such as CO_2/H_2O co-electrolysis, hydrocarbon conversion and ammonia synthesis have been successfully demonstrated by showing promising results, albeit with challenges related to the FE and stability of the systems. Therefore, the efforts should focus beyond the experimental discovery of materials, e.g. on multiscale modelling that would aid optimization of the electrode, electrolyte and their interface, as well as their operating conditions towards enhancing the economic viability of electrosynthesis with PCMRs. Anyhow, the combination of increased number of reported achievements and the necessity of developing sustainable energy storage as well as chemical industry electrification technologies has built an unprecedented momentum for PCMRs which should be capitalized in order to assess their actual capabilities.

Data availability statement

No new data were created or analysed in this study.

Acknowledgments

The authors would like to acknowledge the financial support of the European Innovation Council (EIC) through the ECOLEFINS project (10.3030/101099717) in the context of HORIZON-EIC-2022-PATHFINDEROPEN-01 program. A Z expresses gratitude for the support provided by the Bodossaki Foundation through a scholarship in the 'Stamatis G Mantzavinos' Memorial Postdoctoral Scholarships Programme.

ORCID iDs

Athanasios Zarkadoulas https://orcid.org/0000-0002-0831-0383
Vasileios Kyriakou https://orcid.org/0000-0002-7088-1160

References

[1] Gür T M 2018 Review of electrical energy storage technologies, materials and systems: challenges and prospects for large-scale grid storage *Energy Environ. Sci.* **11** 2696–767
[2] Giddey S, Badwal S P S, Munnings C and Dolan M 2017 Ammonia as a renewable energy transportation media *ACS Sustain. Chem. Eng.* **5** 10231–9
[3] Schiffer Z J, Limaye A M and Manthiram K 2021 Thermodynamic discrimination between energy sources for chemical reactions *Joule* **5** 135–48
[4] Lund P D, Lindgren J, Mikkola J and Salpakari J 2015 Review of energy system flexibility measures to enable high levels of variable renewable electricity *Renew. Sustain. Energy Rev.* **45** 785–807
[5] Rego de Vasconcelos B and Lavoie J-M 2019 Recent advances in power-to-X technology for the production of fuels and chemicals *Front. Chem.* **7** 1–24
[6] Lazkano I, Nøstbakken L and Pelli M 2017 From fossil fuels to renewables: the role of electricity storage *Eur. Econ. Rev.* **99** 113–29
[7] Millet P 2023 11-Electrochemical membrane reactors *Current Trends and Future Developments on (Bio)membranes* ed A Basile and F Gallucci (Elsevier) pp 285–313
[8] Hunt C, Kurimoto A, Wood G, LeSage N, Peterson M, Luginbuhl B R, Horner O, Issinski S and Berlinguette C P 2023 Endergonic hydrogenation at ambient conditions using an electrochemical membrane reactor *J. Am. Chem. Soc.* **145** 14316–23
[9] Vidakovic-Koch T, Gonzalez Martinez I, Kuwertz R, Kunz U, Turek T and Sundmacher K 2012 Electrochemical membrane reactors for sustainable chlorine recycling *Membranes* **2** 510–28
[10] Vayenas C G, Jaksic M M, Bebelis S I and Neophytides S G 1996 The electrochemical activation of catalytic reactions *Modern Aspects of Electrochemistry* vol 29, ed J O Bockris, B E Conway and R E White (Springer) pp 57–202
[11] Tsotsis T T, Minet R G, Champagnie A M and Liu P K 2020 Catalytic membrane reactors *Computer-aided Design of Catalysts* (CRC Press) pp 471–552
[12] Heddrich M P, Gupta S and Santhanam S 2019 Electrochemical ceramic membrane reactors in future energy and chemical process engineering *Chem. Ing. Tech.* **91** 809–20
[13] Stoukides M 2000 Solid-electrolyte membrane reactors: current experience and future outlook *Catal. Rev.* **42** 1–70

[14] Hauch A, Küngas R, Blennow P, Hansen A B, Hansen J B, Mathiesen B V and Mogensen M B 2020 Recent advances in solid oxide cell technology for electrolysis *Science* **370** eaba6118
[15] Liu F, Ding D and Duan C 2023 Protonic ceramic electrochemical cells for synthesizing sustainable chemicals and fuels *Adv. Sci.* **10** 2206478
[16] Min G, Choi S and Hong J 2022 A review of solid oxide steam-electrolysis cell systems: thermodynamics and thermal integration *Appl. Energy* **328** 120145
[17] Nechache A and Hody S 2021 Alternative and innovative solid oxide electrolysis cell materials: a short review *Renew. Sustain. Energy Rev.* **149** 111322
[18] He S, Zou Y, Chen K and Jiang S P 2023 A critical review of key materials and issues in solid oxide cells *Interdiscip. Mater.* **2** 111–36
[19] Hussain S and Yangping L 2020 Review of solid oxide fuel cell materials: cathode, anode, and electrolyte *Energy Transit.* **4** 113–26
[20] Iwahara H, Esaka T, Uchida H and Maeda N 1981 Proton conduction in sintered oxides and its application to steam electrolysis for hydrogen production *Solid State Ion.* **3–4** 359–63
[21] Iwahara H, Uchida H and Maeda N 1982 High temperature fuel and steam electrolysis cells using proton conductive solid electrolytes *J. Power Sources* **7** 293–301
[22] Kreuer K-D 1996 Proton conductivity: materials and applications *Chem. Mater.* **8** 610–41
[23] Haugsrud R and Norby T 2006 Proton conduction in rare-earth ortho-niobates and ortho-tantalates *Nat. Mater.* **5** 193–6
[24] Kreuer K D 1999 Aspects of the formation and mobility of protonic charge carriers and the stability of perovskite-type oxides *Solid State Ion.* **125** 285–302
[25] Kokkofitis C, Ouzounidou M, Skodra A and Stoukides M 2007 High temperature proton conductors: applications in catalytic processes *Solid State Ion.* **178** 507–13
[26] Garagounis I, Kyriakou V, Anagnostou C, Bourganis V, Papachristou I and Stoukides M 2011 Solid electrolytes: applications in heterogeneous catalysis and chemical cogeneration *Ind. Eng. Chem. Res.* **50** 431–72
[27] Duan C, Huang J, Sullivan N and O'Hayre R 2020 Proton-conducting oxides for energy conversion and storage *Appl. Phys. Rev.* **7** 011314
[28] Robinson S, Manerbino A, Grover Coors W and Sullivan N P 2013 Fabrication and performance of tubular, electrode-supported $BaCe_{0.2}Zr_{0.7}Y_{0.1}O_{3-\delta}$ fuel cells *Fuel Cells* **13** 584–91
[29] Chen C, Dong Y, Li L, Wang Z, Liu M, Rainwater B H and Bai Y 2019 High performance of anode supported $BaZr_{0.1}Ce_{0.7}Y_{0.1}Yb_{0.1}O_{3-\delta}$ proton-conducting electrolyte micro-tubular cells with asymmetric structure for IT-SOFCs *J. Electroanal. Chem.* **844** 49–57
[30] Marrony M, Ancelin M, Lefevre G and Dailly J 2015 Elaboration of intermediate size planar proton conducting solid oxide cell by wet chemical routes: a way to industrialization *Solid State Ion.* **275** 97–100
[31] Pirou S, Wang Q, Khajavi P, Georgolamprou X, Ricote S, Chen M and Kiebach R 2022 Planar proton-conducting ceramic cells for hydrogen extraction: mechanical properties, electrochemical performance and up-scaling *Int. J. Hydrog. Energy* **47** 6745–54
[32] Mercadelli E, Gondolini A, Montaleone D, Pinasco P and Sanson A 2021 Innovative strategy for designing proton conducting ceramic tapes and multilayers for energy applications *J. Eur. Ceram. Soc.* **41** 488–96
[33] Clark D *et al* 2022 Single-step hydrogen production from NH_3, CH_4, and biogas in stacked proton ceramic reactors *Science* **376** 390–3
[34] Morejudo S H *et al* 2016 Direct conversion of methane to aromatics in a catalytic co-ionic membrane reactor *Science* **353** 563–6
[35] Duan C *et al* 2018 Highly durable, coking and sulfur tolerant, fuel-flexible protonic ceramic fuel cells *Nature* **557** 217–22
[36] Choi S, Davenport T C and Haile S M 2019 Protonic ceramic electrochemical cells for hydrogen production and electricity generation: exceptional reversibility, stability, and demonstrated faradaic efficiency *Energy Environ. Sci.* **12** 206–15
[37] Yamazaki Y, Blanc F, Okuyama Y, Buannic L, Lucio-Vega J C, Grey C P and Haile S M 2013 Proton trapping in yttrium-doped barium zirconate *Nat. Mater.* **12** 647–51
[38] Quina I, Almar L, Catalán-Martínez D, Dayaghi A M, Martínez A, Norby T, Escolástico S and Serra J M 2023 Direct electrocatalytic CO_2 reduction in a pressurized tubular protonic membrane reactor *Chem. Catal.* **3** 100766
[39] Weng G, Ouyang K, Lin X, Wen S, Zhou Y, Lei S, Xue J and Wang H 2022 Enhanced hydrogen permeability of mixed protonic–electronic conducting membranes through an in-situ exsolution strategy *Adv. Funct. Mater.* **32** 2205255
[40] Chen L, Zhuang L, Xue J, Wei Y and Wang H 2017 Tuning the separation performance of hydrogen permeable membranes using an anion doping strategy *J. Mater. Chem.* A **5** 20482–90
[41] Chen L, Liu L, Xue J, Zhuang L and Wang H 2018 Asymmetric membrane structure: an efficient approach to enhance hydrogen separation performance *Sep. Purif. Technol.* **207** 363–9
[42] Kreuer K D 2003 Proton-conducting oxides *Annu. Rev. Mater. Res.* **33** 333–59
[43] Wang H, Wang X, Meng B, Tan X, Loh K S, Sunarso J and Liu S 2018 Perovskite-based mixed protonic–electronic conducting membranes for hydrogen separation: recent status and advances *J. Ind. Eng. Chem.* **60** 297–306
[44] Marrony M 2015 Proton-conducting oxide materials *Proton-Conducting Ceramics—From Fundamentals to Applied Research* (Jenny Stanford Publishing) pp 73–172
[45] Kyriakou V, Garagounis I, Vourros A, Vasileiou E, Manerbino A, Coors W G and Stoukides M 2016 Methane steam reforming at low temperatures in a $BaZr_{0.7}Ce_{0.2}Y_{0.1}O_{2.9}$ proton conducting membrane reactor *Appl. Catal.* B **186** 1–9
[46] Ricote S, Bonanos N, Manerbino A and Coors W G 2012 Conductivity study of dense $BaCexZr_{(0.9-x)}Y_{0.1}O_{(3-\delta)}$ prepared by solid state reactive sintering at 1500 °C *Int. J. Hydrog. Energy* **37** 7954–61
[47] Choi S, Kucharczyk C J, Liang Y, Zhang X, Takeuchi I, Ji H-I and Haile S M 2018 Exceptional power density and stability at intermediate temperatures in protonic ceramic fuel cells *Nat. Energy* **3** 202–10
[48] Duan C, Kee R, Zhu H, Sullivan N, Zhu L, Bian L, Jennings D and O'Hayre R 2019 Highly efficient reversible protonic ceramic electrochemical cells for power generation and fuel production *Nat. Energy* **4** 230–40
[49] Ding H *et al* 2020 Self-sustainable protonic ceramic electrochemical cells using a triple conducting electrode for hydrogen and power production *Nat. Commun.* **11** 1907
[50] Vøllestad E, Strandbakke R, Tarach M, Catalán-Martínez D, Fontaine M-L, Beeaff D, Clark D R, Serra J M and Norby T 2019 Mixed proton and electron conducting double perovskite anodes for stable and efficient tubular proton ceramic electrolysers *Nat. Mater.* **18** 752–9
[51] Saqib M *et al* 2021 Transition from perovskite to misfit-layered structure materials: a highly oxygen deficient and stable oxygen electrode catalyst *Energy Environ. Sci.* **14** 2472–84
[52] Park K *et al* 2023 Understanding the highly electrocatalytic active mixed triple conducting $NaxCa_{3-x}Co_4O_{9-\delta}$ oxygen electrode materials *Adv. Energy Mater.* **13** 2202999

[53] Almar L, Escolástico S, Navarrete L, Catalán-Martínez D, Ara J, Remiro-Buenamañana S, Quina I and Serra J M 2023 Protonic ceramic electrolysis cells (PCECs) *High Temperature Electrolysis* ed M A Laguna-Bercero (Springer) ch 8, pp 245–76

[54] Bausá N, Escolástico S and Serra J M 2019 Direct CO_2 conversion to syngas in a $BaCe_{0.2}Zr_{0.7}Y_{0.1}O_3$- δ-based proton-conducting electrolysis cell *J. CO_2 Util.* **34** 231–8

[55] Zagoraios D, Panaritis C, Krassakopoulou A, Baranova E A, Katsaounis A and Vayenas C G 2020 Electrochemical promotion of Ru nanoparticles deposited on a proton conductor electrolyte during CO_2 hydrogenation *Appl. Catal.* B **276** 119148

[56] Pan Z, Duan C, Pritchard T, Thatte A, White E, Braun R, O'Hayre R and Sullivan N P 2022 High-yield electrochemical upgrading of CO_2 into CH_4 using large-area protonic ceramic electrolysis cells *Appl. Catal.* B **307** 121196

[57] Liu F, Fang L, Diercks D, Kazempoor P and Duan C 2022 Rationally designed negative electrode for selective CO_2-to-CO conversion in protonic ceramic electrochemical cells *Nano Energy* **102** 107722

[58] Ye Y, Lee W, Pan J, Sun X, Zhou M, Li J, Zhang N, Han J W and Chen Y 2023 Tuning the product selectivity of CO_2/H_2O co-electrolysis using CeO_2-modified proton-conducting electrolysis cells *Energy Environ. Sci.* **16** 3137–45

[59] Choi M, Lee C B, Baek J, Bang S, Hong K, Hong J, Kim K and Lee W 2023 Engineering the surface basicity of heterogeneous catalyst for high Co_2 methanation of protonic ceramic electrolysis cells SSRN 4364666

[60] Malerød-Fjeld H *et al* 2017 Thermo-electrochemical production of compressed hydrogen from methane with near-zero energy loss *Nat. Energy* **2** 923–31

[61] Hua B, Yan N, Li M, Sun Y-F, Zhang Y-Q, Li J, Etsell T, Sarkar P and Luo J-L 2016 Anode-engineered protonic ceramic fuel cell with excellent performance and fuel compatibility *Adv. Mater.* **28** 8922–6

[62] Wang A, Li T, Wang X, Li Z, Huang X, Yin Y, Zhu S, Liu B and Jia L 2023 Enhanced stability of a direct-methane and carbon dioxide protonic ceramic fuel cell with a $PrCrO_3$ based reforming layer *Ceram. Int.* **49** 25240–5

[63] Ding H, Sullivan N P and Ricote S 2017 Double perovskite $Ba_2FeMoO_{6-\delta}$ as fuel electrode for protonic-ceramic membranes *Solid State Ion.* **306** 97–103

[64] Almar L, Bausá N, Fabuel M, Escolástico S and Serra J M 2022 Redox-stable composite electrodes for CH_4 conversion reactors based on proton ceramic electrochemical cells *J. Power Sources* **549** 232048

[65] Liu S, Chuang K T and Luo J-L 2016 Double-layered perovskite anode with in situ exsolution of a Co–Fe alloy to cogenerate ethylene and electricity in a proton-conducting ethane fuel cell *ACS Catal.* **6** 760–8

[66] Shi N, Xue S, Xie Y, Yang Y, Huan D, Pan Y, Peng R, Xia C, Zhan Z and Lu Y 2020 Co-generation of electricity and olefin via proton conducting fuel cells using $(Pr_{0.3}Sr_{0.7})_{0.9}Ni_{0.1}Ti_{0.9}O_3$ catalyst layers *Appl. Catal.* B **272** 118973

[67] Wu W *et al* 2021 Electrochemically engineered, highly energy-efficient conversion of ethane to ethylene and hydrogen below 550 °C in a protonic ceramic electrochemical cell *ACS Catal.* **11** 12194–202

[68] Marnellos G and Stoukides M 1998 Ammonia synthesis at atmospheric pressure *Science* **282** 98–100

[69] Vasileiou E, Kyriakou V, Garagounis I, Vourros A, Manerbino A, Coors W G and Stoukides M 2016 Electrochemical enhancement of ammonia synthesis in a $BaZr_{0.7}Ce_{0.2}Y_{0.1}O_{2.9}$ solid electrolyte cell *Solid State Ion.* **288** 357–62

[70] Klinsrisuk S and Irvine J T S 2017 Electrocatalytic ammonia synthesis via a proton conducting oxide cell with $BaCe_{0.5}Zr_{0.3}Y_{0.16}Zn_{0.04}O_{3-\delta}$ electrolyte membrane *Catal. Today* **286** 41–50

[71] Lei Z, Jing J, Pang J, Hu R, Shi X, Yang Z and Peng S 2020 Highly conductive proton-conducting electrolyte with a low sintering temperature for electrochemical ammonia synthesis *Int. J. Hydrog. Energy* **45** 8041–51

[72] Kyriakou V, Garagounis I, Vourros A, Vasileiou E and Stoukides M 2020 An electrochemical Haber-Bosch process *Joule* **4** 142–58

[73] Sharma R K, Patel H, Mushtaq U, Kyriakou V, Zafeiropoulos G, Peeters F, Welzel S, van de Sanden M C M and Tsampas M N 2021 Plasma activated electrochemical ammonia synthesis from nitrogen and water *ACS Energy Lett.* **6** 313–9

[74] Weng G, Lei S, Wang R, Ouyang K, Dong J, Lin X, Xue J, Ding L-X and Wang H 2023 A high-efficiency electrochemical proton-conducting membrane reactor for ammonia production at intermediate temperatures *Joule* **7** 1333–46

[75] Zhu L, Cadigan C, Duan C, Huang J, Bian L, Le L, Hernandez C H, Avance V, O'Hayre R and Sullivan N P 2021 Ammonia-fed reversible protonic ceramic fuel cells with Ru-based catalyst *Commun. Chem.* **4** 121

[76] He F, Gao Q, Liu Z, Yang M, Ran R, Yang G, Wang W, Zhou W and Shao Z 2021 A new Pd doped proton conducting perovskite oxide with multiple functionalities for efficient and stable power generation from ammonia at reduced Temperatures *Adv. Energy Mater.* **11** 2003916

[77] Hou M, Pan Y and Chen Y 2022 Enhanced electrochemical activity and durability of a direct ammonia protonic ceramic fuel cell enabled by an internal catalyst layer *Sep. Purif. Technol.* **297** 121483

[78] Wang K, Chen H, Li S-D and Shao Z 2022 $SrxTi_{0.6}Fe_{0.4}O_{3-\delta}$ (x = 1.0, 0.9) catalysts for ammonia synthesis via proton-conducting solid oxide electrolysis cells (PCECs) *J. Mater. Chem.* A **10** 24813–23

[79] Guo W, Li Y, Li S-D, Shao Z and Chen H 2024 Ammonia synthesis via a protonic ceramic electrolysis cell (PCEC) using $LaCu_{0.1}Fe_{0.9}O_{3-\delta}$ catalyst *J. Mater. Chem.* A **12** 1200–10

[80] Zhu Z, Zhou M, Tan K, Fan Z, Cao D, Liu Z, Chen M, Chen Y, Chen M and Liu J 2023 High performance and stability enabled by tuning the component thermal expansion coefficients of a proton-conducting solid oxide cell operating at high steam concentration *ACS Appl. Mater. Interfaces* **15** 14457–69

[81] Shi N, Xie Y, Huan D, Yang Y, Xue S, Qi Z, Pan Y, Peng R, Xia C and Lu Y 2019 Controllable CO_2 conversion in high performance proton conducting solid oxide electrolysis cells and the possible mechanisms *J. Mater. Chem.* A **7** 4855–64

[82] Pu T, Tan W, Shi H, Na Y, Lu J and Zhu B 2016 Steam/CO_2 electrolysis in symmetric solid oxide electrolysis cell with barium cerate-carbonate composite electrolyte *Electrochim. Acta* **190** 193–8

[83] Sarabut J, Charojrochkul S, Sornchamni T, Laosiripojana N, Assabumrungrat S, Wetwatana-Hartley U and Kim-Lohsoontorn P 2019 Effect of strontium and zirconium doped barium cerate on the performance of proton ceramic electrolyser cell for syngas production from carbon dioxide and steam *Int. J. Hydrog. Energy* **44** 20634–40

[84] Wu G, Xie K, Wu Y, Yao W and Zhou J 2013 Electrochemical conversion of H_2O/CO_2 to fuel in a proton-conducting solid oxide electrolyser *J. Power Sources* **232** 187–92

[85] Kyriakou V, Athanasiou C, Garagounis I, Skodra A and Stoukides M 2012 Production of C_2 hydrocarbons and H_2 from CH_4 in a proton conducting cell *Solid State Ion.* **225** 219–22

[86] Lei S, Wang A, Weng G, Wu Y, Xue J and Wang H 2023 Simultaneous generation of electricity, ethylene and decomposition of nitrous oxide via protonic ceramic fuel cell membrane reactor *J. Energy Chem.* **77** 359–68

[87] Xue J, Chen Y, Wei Y, Feldhoff A, Wang H and Caro J 2016 Gas to liquids: natural gas conversion to aromatic fuels and chemicals in a hydrogen-permeable ceramic hollow fiber membrane reactor *ACS Catal.* **6** 2448–51

[88] Kyriakou V, Garagounis I, Vasileiou E, Vourros A and Stoukides M 2017 Progress in the electrochemical synthesis of ammonia *Catal. Today* **286** 2–13

[89] Vasileiou E, Kyriakou V, Garagounis I, Vourros A, Manerbino A, Coors W G and Stoukides M 2015 Reaction rate enhancement during the electrocatalytic synthesis of ammonia in a $BaZr_{0.7}Ce_{0.2}Y_{0.1}O_{2.9}$ solid electrolyte cell *Top. Catal.* **58** 1193–201
[90] Li G, Gou Y, Qiao J, Sun W, Wang Z and Sun K 2020 Recent progress of tubular solid oxide fuel cell: from materials to applications *J. Power Sources* **477** 228693
[91] Lei L, Zhang J, Yuan Z, Liu J, Ni M and Chen F 2019 Progress report on proton conducting solid oxide electrolysis cells *Adv. Funct. Mater.* **29** 1903805
[92] Medvedev D 2019 Trends in research and development of protonic ceramic electrolysis cells *Int. J. Hydrog. Energy* **44** 26711–40
[93] Kyriakou V, Garagounis I and Stoukides M 2014 Steam electrolysis with simultaneous production of C_2 hydrocarbons in a solid electrolyte cell *Int. J. Hydrog. Energy* **39** 675–83
[94] Caravaca A, Ferreira V J, de Lucas-consuegra A, Figueiredo J L, Faria J L, Valverde J L and Dorado F 2013 Simultaneous production of H_2 and C_2 hydrocarbons by using a novel configuration solid-electrolyte + fixed bed reactor *Int. J. Hydrog. Energy* **38** 3111–22
[95] Vayenas C G 1988 Catalytic and electrocatalytic reactions in solid oxide fuel cells *Solid State Ion.* **28–30** 1521–39
[96] Kyriakou V, Garagounis I, Vourros A, Marnellos G E and Stoukides M 2018 A protonic ceramic membrane reactor for the production of hydrogen from coal steam gasification *J. Membr. Sci.* **553** 163–70
[97] Wang R, Byrne C and Tucker M C 2019 Assessment of co-sintering as a fabrication approach for metal-supported proton-conducting solid oxide cells *Solid State Ion.* **332** 25–33
[98] Ivanova M E, Escolástico S, Balaguer M, Palisaitis J, Sohn Y J, Meulenberg W A, Guillon O, Mayer J and Serra J M 2016 Hydrogen separation through tailored dual phase membranes with nominal composition $BaCe_{0.8}Eu_{0.2}O_{3-\delta}$:$Ce_{0.8}Y_{0.2}O_{2-\delta}$ at intermediate temperatures *Sci. Rep.* **6** 34773
[99] Abghoui Y, Garden A L, Howalt J G, Vegge T and Skúlason E 2016 Electroreduction of N_2 to ammonia at ambient conditions on mononitrides of Zr, Nb, Cr, and V: a DFT guide for experiments *ACS Catal.* **6** 635–46
[100] Du H-L, Chatti M, Hodgetts R Y, Cherepanov P V, Nguyen C K, Matuszek K, MacFarlane D R and Simonov A N 2022 Electroreduction of nitrogen with almost 100% current-to-ammonia efficiency *Nature* **609** 722–7